

Geochemistry, Geophysics, Geosystems

RESEARCH ARTICLE

10.1029/2018GC008027

Special Section:

Carbon degassing through volcanoes and active tectonic regions

Key Points:

- Melt inclusion geochemistry indicates that the melts supplying Mt. Etna are heterogeneous with respect to trace and volatile elements
- Melts may be influenced by crustal carbonate assimilation or by recycled plagioclase-rich cumulates in the mantle
- Rapidly rising melts at Etna may become supersaturated in volatiles, causing a burst of shallow degassing, which may trigger eruptions

Supporting Information:

- Supporting Information S1

Correspondence to:

M. Edmonds,
marie.edmonds@esc.cam.ac.uk

Citation:




Salem, L. C., Edmonds, M., Corsaro, R. A., & Maclennan, J. (2019). Carbon dioxide in geochemically heterogeneous melt inclusions from Mount Etna, Italy. *Geochemistry, Geophysics, Geosystems*, 20. <https://doi.org/10.1029/2018GC008027>

Received 26 NOV 2018

Accepted 25 APR 2019

Accepted article online 3 JUN 2019

Carbon Dioxide in Geochemically Heterogeneous Melt Inclusions From Mount Etna, Italy

L. C. Salem¹ , M. Edmonds¹ , R. A. Corsaro², and J. Maclennan¹ 

¹Department of Earth Sciences, University of Cambridge, Cambridge, UK, ²Osservatorio Etneo, Sezione di Catania, Istituto Nazionale di Geofisica e Vulcanologia, Catania, Italy

Abstract Mt. Etna is among the largest global volcanic outgassers with respect to carbon and sulfur, yet questions remain regarding the source of these volatiles and their systematics in the crust and mantle. The importance of heterogeneous mantle sources, mixing, crustal assimilation, and disequilibrium degassing is investigated using melt inclusions erupted during the CE 1669 eruption of Mt. Etna, Italy. We find that the melt inclusion compositions define a mixing array between two geochemically distinct melts. One end-member melt is depleted in light rare Earth elements (LREEs) and enriched in strontium (Sr), carbon, and sulfur; the other is enriched in LREE and depleted in Sr, carbon, and sulfur. We infer, through modeling, that the melts may either have been generated by melting a mantle source that includes a recycled oceanic crustal component or they may have assimilated carbonate material in the crust. The resulting LREE-depleted, Sr-enriched melts were also alkali-rich, which enhanced the solubility of carbon and sulfur. The LREE-depleted, Sr- and volatile-rich melt ascended through the crust and likely became supersaturated with respect to CO₂ and sulfur. The melt intruded into a LREE-enriched, relatively degassed magma body in the shallow crust, cooled rapidly, and vesiculated, likely triggering eruption. The melt inclusion array trapped by growing olivines during this intrusion process records a snapshot of incomplete mixing between the two melts. Mt. Etna is renowned for the large increases in CO₂ gas fluxes shortly before and during eruption. The intrusion of supersaturated, CO₂-enhanced magmas into shallow reservoirs may be a common process at Mt. Etna.

1. Introduction

Mt. Etna, Italy, is one of the most prolific volcanic outgassers (Aiuppa et al., 2006; Allard et al., 1991; Gerlach, 1991; Halmer et al., 2002), supplying almost 10% of the global volcanic output of carbon dioxide (CO₂) annually (Burton et al., 2013). Explosive eruptions of Mt. Etna over the past decade have been preceded by increases in the CO₂ gas flux from the volcano, perhaps caused by the migration of CO₂-rich exsolved fluids ahead of the ascending magma (Aiuppa et al., 2006; Aiuppa et al., 2007). Melt inclusion studies have shown that CO₂-rich fluids may segregate at deep levels and flush melts stored in shallow reservoirs (Andronico & Corsaro, 2011; Collins et al., 2009; Métrich et al., 2004; Spilliaert et al., 2006). The water (H₂O) and CO₂ content of melt inclusions has been used—assuming the melts are vapor-saturated and have degassed in equilibrium—to estimate pressures of melt inclusion entrapment of 150 to 400 MPa (Corsaro et al., 2014; Spilliaert et al., 2006; Spilliaert, Allard, et al., 2006). The large scatter in the CO₂ concentrations, which deviate greatly from equilibrium closed system degassing paths (in common with many melt inclusion volatile data sets; Métrich & Wallace, 2008), has been ascribed to a wide range of processes including gas fluxing, mixing, and postentrapment processes (Bucholz et al., 2013; Gaetani et al., 2012; Hartley et al., 2014; Maclennan, 2017; Sides et al., 2014; Wallace et al., 2015). The origin of the carbon has been debated. Its isotopic composition, expressed as δ¹³C, ranges from -4.5 to -1.0‰ (Allard et al., 1991; Chiodini et al., 2010). This isotopic composition suggests either a heterogeneous and relatively heavy carbon reservoir in the mantle that was recycled during subduction (Frezza et al., 2009) or a mixture between MORB-like mantle carbon and a heavier crustal limestone component (Chiodini et al., 2010; Marziano et al., 2008; Mason et al., 2017; Mollo et al., 2010). The trace element compositions of primitive melt inclusions suggest that the melts supplying Mt. Etna are heterogeneous, implying not only different degrees of melting but also a highly enriched mantle source that was influenced by subduction fluids (Correale et al., 2014; Kamenetsky et al., 2007; Schiavi et al., 2015; Viccaro & Cristofolini, 2008).

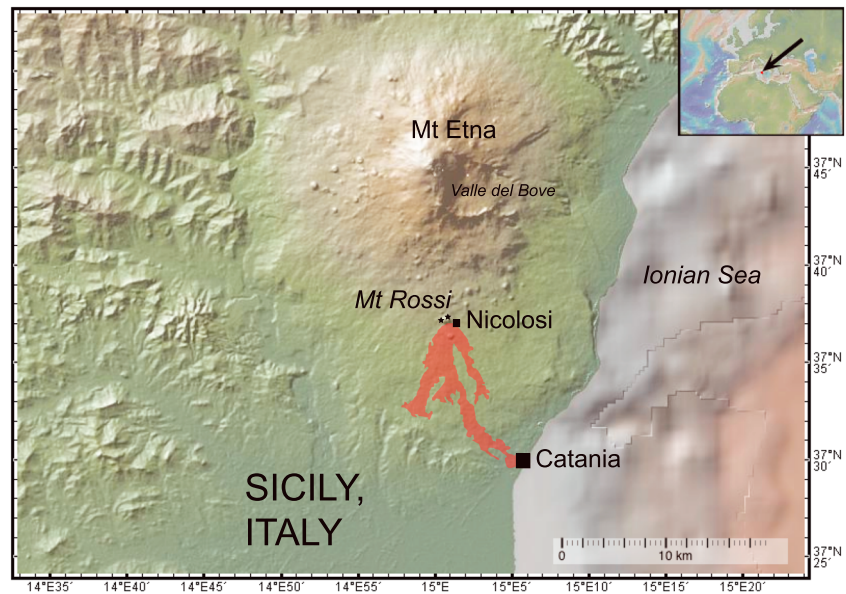


Figure 1. Map of Mt. Etna with 1669 Monti Rossi scoria cone indicated. Lava flows from Monti Rossi cone to Catania are indicated in red from (Branca et al., 2013) and sample sites at Monti Rossi cone are shown by black stars (SW and NE sides of cone). Map produced using *Geomapapp* (<http://www.geomapapp.org>) using the Global Multi-Resolution Topography (GMRT) Synthesis (Ryan et al., 2009).

In this study, the geochemistry of melt inclusions in tephra produced by the historic CE 1669 eruption is examined. This eruption was the largest of the past 500 years at Mt. Etna (Branca & Ferrara, 2013; Corsaro et al., 1996) and one that marked a significant change in both the style of eruption and the composition of lavas (Mulas et al., 2016). A combination of microanalytical techniques are used to constrain the major, trace, and volatile element chemistry of melts trapped in olivine phenocrysts and to model processes that affect melt batches and fractionate their chemistry. In particular, we seek to deconvolve the processes affecting the differentiation of the melt feeding the volcanic system at Mt. Etna, how CO_2 and sulfur concentrations vary with trace element compositions, and consequently whether CO_2 is sourced from crustal carbonate or from the mantle. In doing so, the integrity of the melt inclusions is tested along with the assumption of equilibrium degassing of melts feeding Mt. Etna, Italy. These results have implications for the interpretation of pulses of CO_2 gas flux prior to eruptions (Aiuppa et al., 2007).

2. Geological Setting

Mt. Etna (Sicily, Italy) is the largest active volcano in Europe and one of the most persistently active volcanoes globally (Figure 1). It is situated at the intersection of several major fault systems associated with the subduction of the African plate beneath the Eurasian plate (Doglioni et al., 2001; Gvirtzman & Nur, 1999), yet its lavas are geochemically similar to ocean island basalts (Montelli et al., 2006; Schiano et al., 2001; Schiavi et al., 2015; Tanguy et al., 1997). Melts originate in the asthenosphere (Schiavi et al., 2015) and interact with thick lithospheric mantle (Corsaro et al., 2014; Marty et al., 1994) and carbonate- and cumulate-bearing crust (Correale et al., 2014; Corsaro et al., 2009). Mt. Etna rests upon a subvolcanic sedimentary basement made of marls and clays, limestones, and terrigenous sedimentary rocks (~2 km thick) that form the Maghrebian-Appennine Chain (Catalano et al., 2004). These sediments overlie the Hyblean Plateau, a Mesozoic to Mid-Pleistocene carbonate succession of limestone and dolomite (Pedley & Grasso, 1992), which begins at a depth of ~5 km and has an average thickness of about 10 km and may interact thermally with rising magmas (Heap et al., 2013). Despite the occurrence of variably altered carbonate xenoliths, particularly in the lavas erupted in 1989 (Michaud, 1995), and heavy carbon isotopes in volcanic gases that has been linked to carbonate assimilation (Chiodini et al., 2011; Mason et al., 2017), petrological and geochemical evidence for direct carbonate assimilation has been lacking.

Lavas erupted from Mongibello, the most recent (15 ka to present) volcanic edifice of the Etnean succession, belong to a mildly alkaline series and have compositions that are variable from trachybasalt to benmoreite (Corsaro & Pompilio, 2004, and references therein). Most products are sodic (hawaiites), but since the 1970s, there has been a shift toward a more potassic affinity (K-trachybasalts), with varying degrees of K-enrichment. Petrological data and geophysical evidence suggest that Mt. Etna's plumbing system is complex. A highly porphyritic plagioclase-rich, K-trachybasalt is the most commonly erupted magma during both summit and flank eruptions, ascending from a shallow storage region (<5 km below sea level). There is also infrequent eruption of nearly aphyric basaltic magma that may ascend directly from a deeper region (10-12 km below sea level) of the plumbing system. In the last 50 years this magma has erupted in 1974 (Bottari et al., 1975; Corsaro et al., 2009; Tanguy et al., 1997), 2001 (Corsaro et al., 2007; Métrich et al., 2004) and 2002-2003 (Andronico et al., 2005; Spilliaert, Allard, et al., 2006). Geophysical evidence suggests that magma reservoirs exist at 1 to 5-km and 10- to 15-km depth where there are cumulates and dyke structures, as indicated by seismic high-velocity bodies (Aloisi et al., 2002; Hirn et al., 1991; Patanè et al., 2006) and recent petrological studies (Corsaro et al., 2014). There is also evidence, for some eruptions, of deeper melt storage close to the Moho (e.g., from crystallization of pyroxene before plagioclase in the 1974 lavas; Tanguy & Kieffer, 1977).

Mt. Etna is an important global source of volcanic gases rich in sulfur and carbon, with annual CO₂ fluxes of up to 6×10^9 kg per year (Burton et al., 2013). Much of this carbon outgassing flux occurs between eruptions (Allard et al., 1991). Previous melt inclusion studies have shown that the melts contain at least 0.3 wt.% sulfur at 140 MPa (from H₂O-CO₂ barometry) and magmas are fluxed with CO₂-rich magmatic vapor (Allard et al., 2006; Collins et al., 2009; Ferlito et al., 2008; Spilliaert, Allard, et al., 2006). The vapor may precede the transport of magma to the surface on a timescale from days to weeks (Aiuppa et al., 2007; Aiuppa et al., 2008).

The CE 1669 eruption, which began on 11 March and lasted for four months, was the largest and most destructive in historical times, largely due to the relatively low elevation of the vents (the main scoria cone, Monti Rossi, is at 800 m above sea level; Figure 1), the large volume of lava erupted ($607 \pm 105 \times 10^6$ m³; Branca et al., 2013) and the high average effusion rate of 58 m/s. The lava flowed 17 km from the vent, impacting a densely populated area and partly destroying Catania (Figure 1; Branca et al., 2013). Strombolian activity initially produced a large, 1-km-wide, and 200-m-high, scoria cone (Figure 1) and a thick, widespread pyroclastic fall deposit along the lower south-east flank of the volcano (Mulas et al., 2016). The total tephra fall volume, including the Monti Rossi cone, is estimated to be 6.6×10^7 m³ (about 3.2×10^7 -m³ dense rock equivalent; Mulas et al., 2016). Later, the eruption produced a wide 'a'a flow-field (Branca et al., 2013; Branca & Vigliotti, 2015).

Lavas erupted early in the CE 1669 eruption (denoted "SET1" by Corsaro et al., 1996) are more primitive than those erupted during the later stages of the eruption ("SET2"). Throughout the eruption the bulk rock mean MgO content decreases from a mean of 6.65 to 5.07 wt.% (Corsaro et al., 1996). This change in bulk composition has been interpreted as evidence for fresh mafic magma intruding into a shallow reservoir containing more evolved magma (Corsaro et al., 1996). However, a more recent study of 1669 lavas has shown that lavas erupted before 29 March 1669 (i.e. SET1) are geochemically similar to lavas erupted after 29 March 1669 (i.e., SET2), and both are similar to the Monti Rossi scoria compositions reported by Mulas et al. (2016). The significantly higher Al₂O₃, SiO₂, and total alkalis of the SET2 reported by Corsaro et al. (1996) are proposed to be due to plagioclase accumulation (Kahl et al., 2017). The Monti Rossi cone, which we sample and analyze here, was formed rapidly, largely over the first 2 days of the eruption: 11 and 12 March 1669 (Mulas et al., 2016; equivalent to the SET1 of Corsaro et al., 1996, and Kahl et al., 2017).

A study of core to rim olivine compositions from the SET1 and SET2 lavas demonstrated more complex syneruptive and preeruptive environments (Kahl et al., 2017). Olivine cores in the SET1 lavas (which are similar to the Monti Rossi tephras; Mulas et al., 2016) have a composition of Fo₇₅₋₇₈ and are inferred to have formed in a partially degassed environment together with clinopyroxene (Mg# 81-83), plagioclase (An₆₆₋₇₅), and Fe-Ti oxides (Mt₃₅₋₅₂), at a temperature of ~1170 °C and pressures of <1 kbar (Kahl et al., 2017). The olivine cores define a compositional plateau formed under relatively uniform conditions, whereas the olivine rims (Fo₅₁₋₅₉) define a broad compositional range that may form over a broad pressure range <1 kbar. The

SET2 lavas, erupted later in the eruption (not studied in the current work), contain olivines with similar composition cores, and much less evolved rims (Fo_{65-69}). Three distinct magma reservoirs located in the volcano's shallow plumbing system and several events of magma recharge have been proposed, based on studies of these olivines, in the 1.5 years leading up to the eruption, with the SET1 and SET2 magmas being derived from a distinct, bifurcated feeding dyke system (Kahl et al., 2017).

The CE 1669 eruption marked a significant change in the geochemical and eruptive regime of Mt. Etna (Clocchiatti et al., 1988; Condomines et al., 1995). From CE 1600 to 1669, volcanic activity was frequent, long-lasting, and of high-volume effusive eruptions of plagioclase-phyric lavas. In contrast, the period CE 1670-1750 was characterized by sporadic and shorter eruptions with low effusion rates and more mafic lavas. This eruption provides an opportunity to observe a large spectrum of geochemically diverse melts at a critical point in Mt. Etna's recent history and to understand how this melt heterogeneity maps on to volatile systematics.

3. Sampling and Analytical Techniques

Glassy tephra was sampled from two localities (north-east: NEMR and south-west: SWMR) at the base of the main scoria cone, Monti Rossi, in Nicolosi on the South-East flank of Mt. Etna (Figure 1), from the MR1 unit of Mulas et al. (2016). The scoria cone was erupted over the first 2 days of the eruption (Corsaro et al., 1996; Kahl et al., 2017; Mulas et al., 2016). Melt inclusions with included oxide crystals were analyzed but showed no systematic trend in major or trace element concentration with oxide-free MIs (Figure S1 in the Supporting Information), suggesting that they may be "pre-entrapment" phases. Crystals were individually mounted in CrystalBond and polished to expose melt inclusions before being remounted in Buehler EpoThin resin and repolished for analysis. The 31 melt inclusions analyzed in this study are without cracks or shrinkage bubbles (Figure 2). We note that avoiding melt inclusions with shrinkage bubbles may bias the data set; it is possible that we may miss an earlier population of melt inclusions, for example (i.e., prior to any pre-eruptive mixing).

Trace elements, F, H_2O , and CO_2 , were analyzed by secondary ion mass spectrometry (SIMS) using a Cameca ims-4f instrument at the Natural Environment Research Council Ion Microprobe Facility at the University of Edinburgh, UK. CO_2 analyses were performed first, with a high mass resolution configuration, in order to enable good separation of C and Mg peaks. H_2O , F, and trace elements were then measured with a lower mass resolution configuration. Errors in CO_2 and H_2O were assessed using repeat analyses of a suite of basaltic glass standards (Pichavant et al., 2009). Precision for H_2O and CO_2 was 1%. Average accuracy, expressed as % recovery of published compositions determined by FTIR, was 100.6%. NIST-610 was used as the calibration standard for trace element analyses (Jochum et al., 2011). Accuracy was monitored by analysis of international standards, NIST-610 and BCR-2G throughout analytical sessions. The accuracy of published compositions, relative to NIST-610 and BCR-2G standards (Jochum et al., 2005; Jochum et al., 2011; given by $|(100 - A)|$, where A is the % recovery (given by the unknown determination divided by the known values, expressed as a %; Table S1 in the supporting information), was <16% for all trace elements and <5% for most trace elements (Table S1). Precision was estimated as 1 standard deviation relative error and varied between 0.1% (Ce) and 15.8% (Eu) using repeat analyses of BCR-2G (Jochum et al., 2011). Precision was calculated for trace element ratios and volatile/trace ratios using repeat analyses of the same standards. One percentage relative error (in parentheses) was calculated for La/Yb (0.5), Ce/Y (2.9), CO_2/Nb (0.9), and $\text{H}_2\text{O}/\text{Ce}$ (1.1).

Major elements, S and Cl, were determined by electron probe microanalysis (EPMA) using a Cameca SX100 instrument at the Department of Earth Sciences at the University of Cambridge, UK. Full details of the analytical setup for SIMS and EPMA and error analysis are detailed in the Table S1.

Signal-to-noise ratios were calculated for all elements analyzed in order to assess the contribution of natural variation and analytical error to the generation of sample variability. The method described in MacLennan et al. (2003) was used:

$$\sigma_t^2 = \sigma_0^2 - \sigma_r^2$$

where σ_t is the true variation of the sample set, σ_0 is the observed variation, and σ_r is an estimate of analytical error. The χ^2 distribution was used to assess the quality of σ_r , which depends on the number of repeat

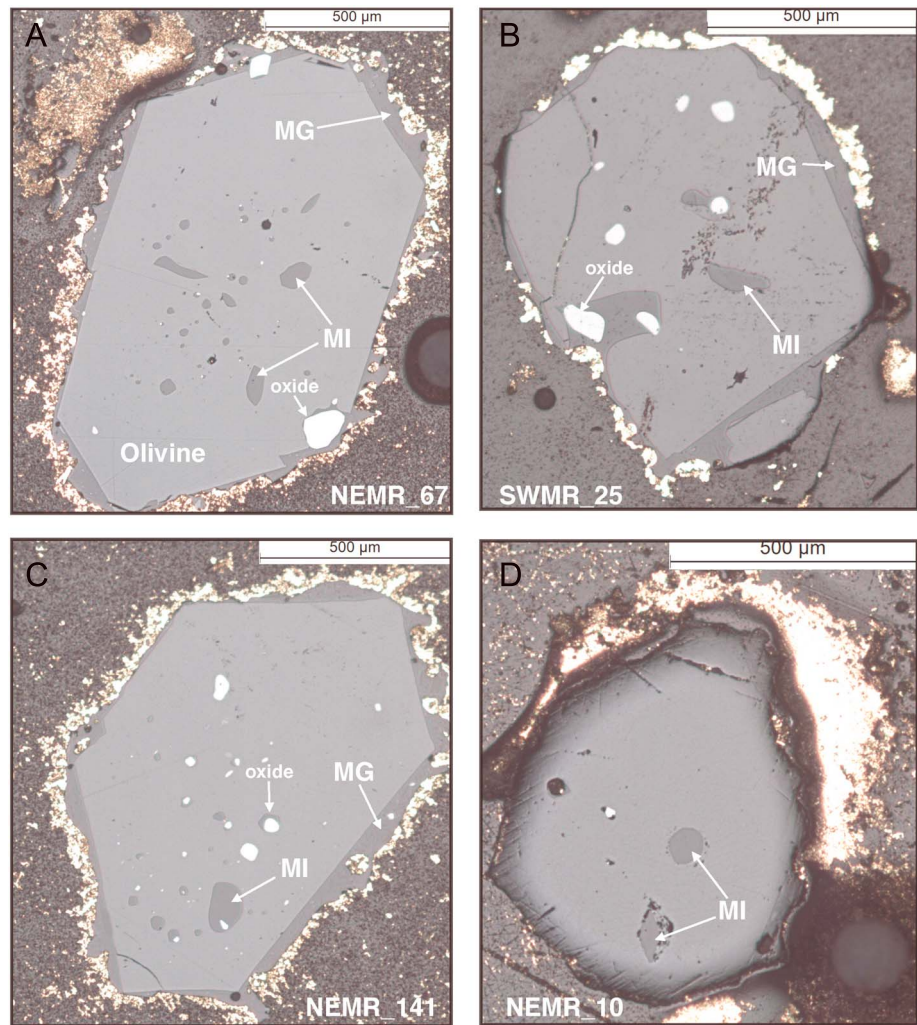


Figure 2. Photomicrographs of olivine crystals with melt inclusions (MI), oxide inclusions, and matrix glass in samples: (a) NEMR 67, (b) SWMR 25, (c) NEMR 141, and (d) NEMR 10. 500- μm scale bar marked.

analyses to estimate analytical precision, in order to test whether signal-to-noise ratios are significant at a given confidence level. Signal-to-noise ratios for all major and trace elements in glass are greater than the threshold for significant variability at the 99% confidence interval. Signal-to-noise ratios are high for incompatible and abundant elements. For example, Sr has a signal-to-noise ratio of $\sigma_i/\sigma_r = 11.5$, whereas Nd, which is less abundant, has $\sigma_i/\sigma_r = 2.2$ and Nb, which is more incompatible has $\sigma_i/\sigma_r = 4.8$. Elements that were analyzed with low precision have low signal-to-noise ratios, such as Gd ($\sigma_i/\sigma_r = 0.5$), and it is not possible to resolve natural variability through analytical noise.

4. Results

4.1. Crystal Assemblage

The crystallinity of the tephra samples was estimated to lie in the range 10 to 25 vol.% (consistent with the “porphyricity” measured for the lava samples, which ranges from 21 to 30 vol%; Kahl et al., 2017), with olivine, plagioclase (which makes up 60–80 vol.% of the crystals), augite, and titanomagnetite. This crystal assemblage is consistent with other recent studies of the 1669 eruption lava flows (Corsaro et al., 1996; Kahl et al., 2017). Host core olivine compositions fall within a narrow range, Fo_{73-76} (see the supporting information) overlapping the olivine compositions of the two dominant groups (Type IV and VII) of Kahl et al. (2017). Matrix glass magnesium numbers (Mg#) range from 37 to 42. The olivine cores are in general

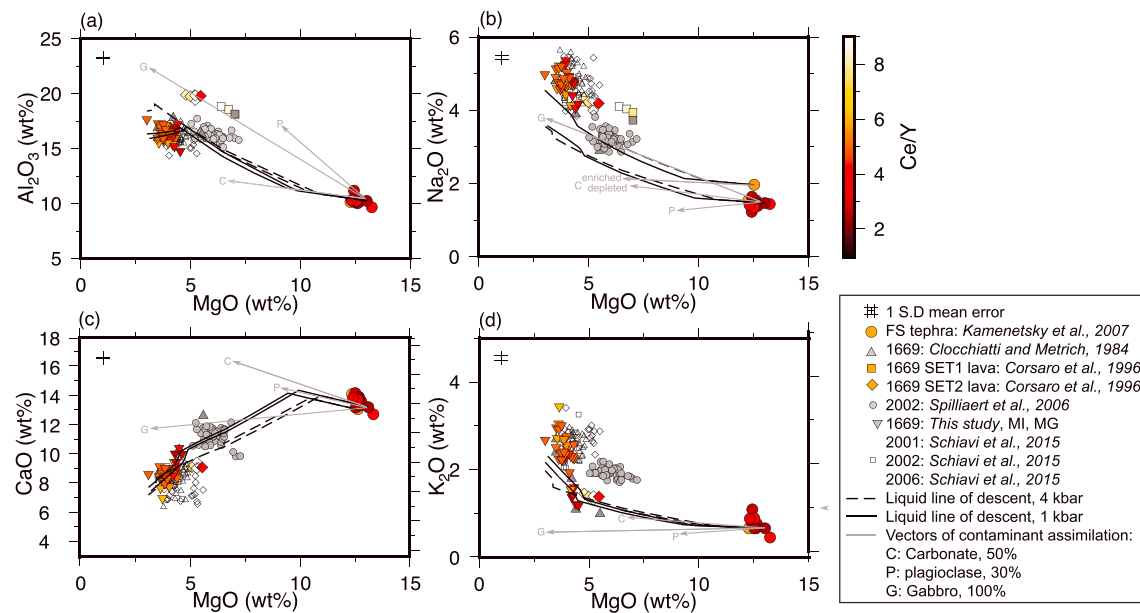


Figure 3. Major element oxide (wt. %) compositions for CE 1669 MI and MG (this study) compared to (i) 3930±60 B.P. (4 kyr) Fall-Stratified basalts (FS) MI (Kamenetsky et al., 2007), (ii) previous CE 1669 MI study (Clocchiatti & Metrich, 1984), (iii) CE 1669 WR lavas (Corsaro et al., 1996), (iv) 2002 MI (Spilliaert, Allard, et al., 2006), and (v) 2001, 2002, 2006 MI (Schiavi et al., 2015). Symbols distinguish different studies. The dashed line represents the modeled fractional crystallization path using the two end-member primitive FS melts at 1 kbar (solid line) and 4 kbar (dashed line) with Petrolog3 software (Danyushevsky & Plechov, 2011). Color bar scales for Ce/Y, a measure of degree of LREE-enrichment. Vectors represent assimilation of contaminants (Carbonate - C, Plagioclase - P, and Gabbro - G) by the two end-member FS melts, adapted from Carter and Dasgupta (2015) and Mollo et al. (2010).

too forsteritic to be in equilibrium with the carrier liquid using a K_d of ~0.30, where K_d is equal to

$$\left(\frac{x_{\text{Fe}^{2+}}}{x_{\text{Mg}}} \right)_{\text{ol}} / \left(\frac{x_{\text{Fe}^{2+}}}{x_{\text{Mg}}} \right)_{\text{liq}} \quad (\text{Roeder \& Emslie, 1970; Figure S6}).$$

4.2. Melt Inclusion Major Element Composition

Melt inclusion compositions may be modified by post-entrapment crystallization (PEC). The extent of PEC was estimated using Petrolog3 in reverse fractional crystallization mode, which accounts for Fe-Mg diffusion between the host olivine and the melt inclusion (Danyushevsky & Plechov, 2011), and it was found that all inclusions experienced 5-10% PEC. This affects the MgO and FeO of the melt inclusion, and thus, the Mg# is recalculated to 45-51 (shown in Table S5). The Mg# was calculated for the matrix glass and melt inclusions using only Fe, assuming that FeO is 0.70 to 0.85 Fe (Metrich & Clocchiatti, 1989; Table S5). The major element compositions of the melt inclusions are K-poor trachybasaltic, typical of pre-1970 lavas and similar to the plagioclase-rich and K-poor products of the 1763 eruption (Corsaro et al., 2009). Major element oxide compositions are within the field for post-1500 Etnean lavas (Corsaro et al., 1996; Cristofolini & Romano, 1982) and recent 21st century eruption melt inclusion analyses (Figure 3; Collins et al., 2009; Métrich et al., 2004; Schiavi et al., 2015; Spilliaert, Allard, et al., 2006) but far more evolved than the olivine-hosted MI from the 4-kyr Fall Stratified eruption at Mt. Etna (hereafter FS; Kamenetsky et al., 2007), considered one of the most primitive melts erupted at Mt. Etna.

4.3. Melt Inclusion Trace Element Composition

The melt inclusions are relatively enriched in incompatible trace elements compared to N-MORB. The trace element patterns normalized to primitive mantle (PM) for melt inclusions and matrix glasses display greater enrichment in light rare Earth element (LREE) and Nb than heavy rare Earth element (HREE; Figure 4). Concentrations of Nb in the 1669 melt inclusions range from 50 to 140 ppm, La 60-140 ppm, and Nd 50-100 ppm (Figure 5a), 2-3 times greater than the primitive FS MI measured by (Kamenetsky et al., 2007; Figure 5, colored circles), but within the range of recent eruptions in 2001-2007 (Collins et al., 2009;

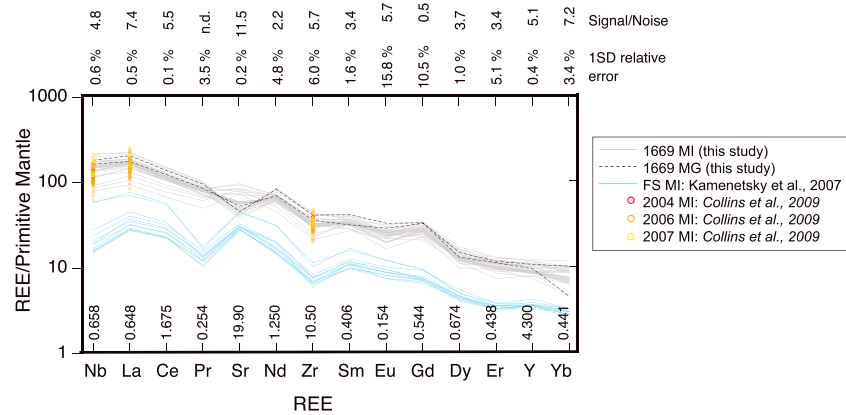


Figure 4. Trace element profile for this study of CE 1669 melt inclusions (MI: fine gray line), 1669 matrix glass (MG: black dashed lines) compared to (i) 3930±60 B.P. Fall Stratified (FS) eruption MI (blue line; (Kamenetsky et al., 2007)) and (ii) 2004, 2006, 2007 eruption MI (colored circles; (Collins et al., 2009)). All concentrations are normalized to primitive mantle (McDonough & Sun, 1995).

Schiavi et al., 2015). Ce/Y varies between 2 and 6 (Figure 5b) similar to the range in both the FS MI (Kamenetsky et al., 2007) and 2001-2006 melt inclusions (Schiavi et al., 2015). CE 1669 matrix glass compositions also lie within this range (gray inverse triangles). The most enriched melt inclusions (with highest LREE/HREE ratios) are also those with the highest absolute concentrations of LREE (Figure 5a). The full suite of crystals host compositionally variable melts with Ce/Y ratios between 2 and 6, which is independent of the host olivine composition for both the CE 1669 MI and FS (Figure S2). It is worthy of

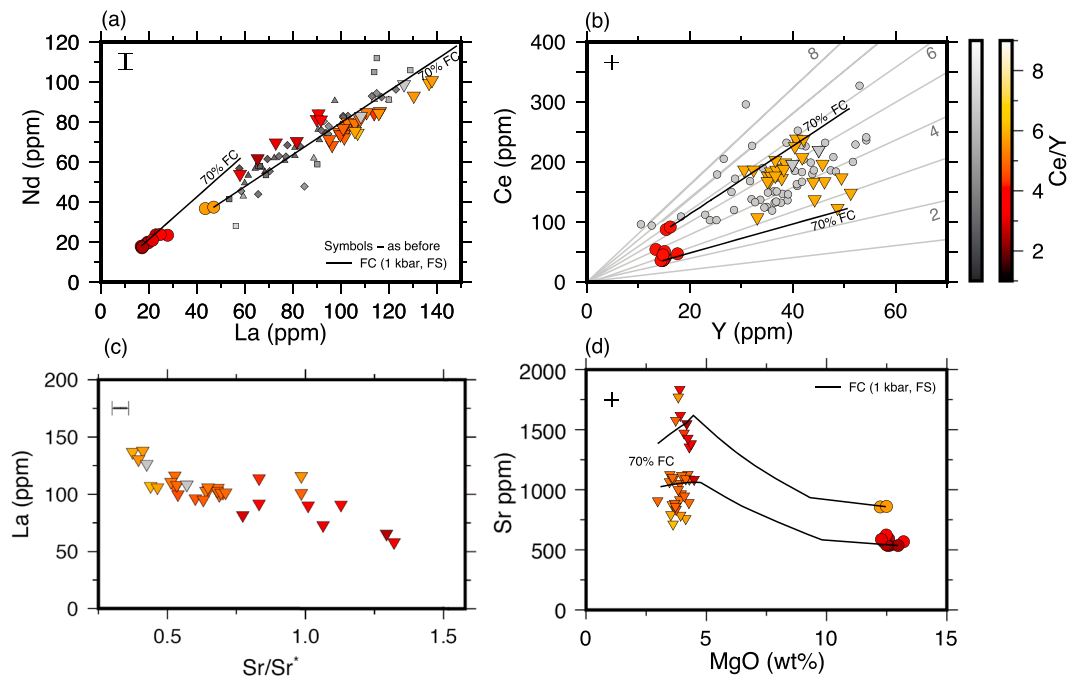


Figure 5. (a) Nd and La trace element concentrations (ppm) for CE 1669 MI (this study) compared to (i) 3930 60 B.P. Fall-Stratified (FS) basalts MI (Kamenetsky et al., 2007); (ii) 2001-2006 MI (Schiavi et al., 2015). Symbols as before. The solid black line represents modeled fractional crystallization (FC) path using two end-member primitive FS MI at 1 kbar and Petrolog3 software (Danyushevsky & Plechov, 2011). Color bars scale for Ce/Y, a measure of degree of LREE-enrichment: CE 1669 and FS: red-yellow, 2001-2006: gray-scale. (b) Ce against Y (ppm) for the same MI studies as (a) with gray lines of constant Ce/Y ratio and solid black lines as before. (c) La against Sr for 1669 MI showing negative correlation between Sr and LREE. (d) Sr against MgO showing breadth of Sr concentration in CE 1669 samples at a limited MgO wt.%. Solid black line as before.

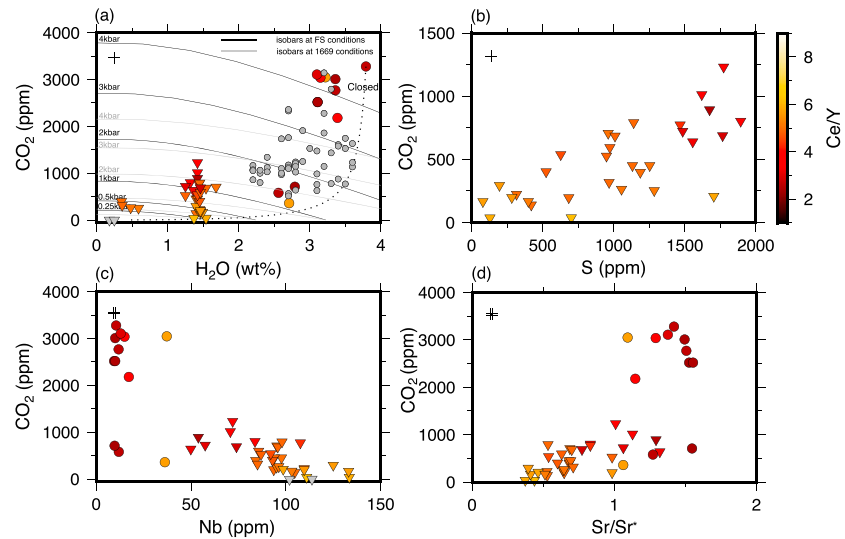


Figure 6. (a) Melt H₂O against CO₂ with closed (dotted lines) system degassing modeled from primitive Fall-Stratified (FS) melt compositions using SolEx (Witham et al., 2012). Isobars marked (SolEx) for both FS conditions (solid black line) and 1669 conditions (solid gray line). Symbols as before for CE 1669 MI and MG (this study), 2002 MI (Spilliaert, Allard, et al., 2006) and FS (Kamenetsky et al., 2007) MI. (b) Positive correlation of CO₂ against sulfur in 1669 MI. Symbols and color bar as before. (c) Negative correlation of CO₂ against Nb in 1669 MI and MG. Symbols and color bar as before. FS MI does not follow the same correlation. (d) CO₂ against Sr anomaly (Sr/Sr). Sr* calculated from the relative compatibility of neighboring REE Ce and Nd, see text for details of calculation.

note that the trace element diversity in the melt inclusions far exceeds the diversity in whole rock compositions for the SET1 lavas, for which Ce/Y only varies by ~ 3% and K₂O only from 1.3 to 1.6 wt% (Mulas et al., 2016).

A correlation coefficient matrix reveals broad-scale correlation trends in the data (Figure S3). Ba, La, Nb, Ce, Pr, Nd, and Zr show strong positive correlations with each other ($r > 0.9$) but a weak negative correlation with HREE and Y ($r = -0.2$), suggesting that the primary melts were generated from sources with variable LREE-enrichment or from variable degrees of fractional melting at a pressure where garnet is present to fractionate HREE from LREE. Sr shows a weak negative correlation with the LREE ($r = -0.4$; Figure 5c) and a positive correlation with HREE ($r = 0.3$; Figure S3).

MI show varying degrees of Sr enrichment and depletion from the expected concentration (Sr). Sr is determined using the relative compatibility of the neighboring REE in order of compatibility, Ce and Nd, using $Sr^* = \left[\frac{[Ce]_{MI}}{[Ce]_{PM}} * \frac{[Nd]_{MI}}{[Nd]_{PM}} \right]^{1/2}$, where (Ce) and (Nd) are the concentration of these elements in either MI or PM (Sobolev & Nikogosian, 1994). $Sr/Sr^* > 1$ suggests enrichment in Sr compared to the expected concentration based on compatibility, and $Sr/Sr^* < 1$ suggests depletion in Sr. All FS melts have $Sr/Sr^* > 1$, and Sr enrichment is greatest for the relatively LREE-depleted 1669 melts. Sr depletion scales with LREE-enrichment and increasing LREE/HREE ratios (Figures 5c and S4). Enrichment in fluid mobile elements, such as Ba, appears to correlate with LREE-enrichment but not with Sr enrichment (Figure S3).

4.4. Melt Inclusion Volatile Systematics

H₂O concentrations in the 1669 melt inclusions exhibit a limited variability, with a range of 1.2-1.7 wt.% H₂O and a median of 1.4 wt.% (Figure 6a). Matrix glasses contain <0.6 wt.% H₂O. The limited range and low values reflect either their entrapment pressure or their diffusive equilibration during storage at low pressures (70-100 MPa) in the crust (Bucholz et al., 2013; Gaetani et al., 2012). H₂O concentrations may be reset to low-pressure conditions by diffusive reequilibration and may therefore be unrepresentative of their entrapment pressure.

CO₂ concentration in the melt inclusions varies from 40 to 1,220 ppm; CO₂ concentrations in matrix glasses are below detection (20 ppm; gray triangles, Figure 6a). Sulfur concentrations in the melt inclusions vary between 80 and 1,900 ppm (Figure 6b). Carbon and sulfur in melt inclusions correlate well ($r = 0.73$,

Figures 6b and S3). Perhaps the most striking feature, however, of the covariance structure for the CE 1669 melt inclusion geochemistry is that CO₂ and sulfur both correlate negatively with incompatible elements such as Nb, LREE, Ba, and Zr (Figure 6c). For the CE 1669 data alone, the correlation between CO₂ and Nb, for example, has an r value of -0.68 (CO₂ and, e.g., Ce, $r = -0.59$; Ba, $r = -0.51$; and Zr, $r = -0.59$; Figure S3). The most CO₂-rich and S-rich melts are those with lowest Ce/Y, and Ce/Y shows a negative correlation with CO₂ and S with r values of -0.77 and -0.70, respectively. CO₂, however, correlates well with Sr and Sr/Sr* ($r = 0.63, 0.67$, respectively; Figures 6d and S3). Fluorine shows a high degree of variability (0.14–0.24 wt.%) with no correlation with either host olivine Fo mol% or degree of melt enrichment. Chlorine shows moderate variability (0.16–0.38 wt.%) with a weak negative correlation with LREE enrichment ($r = -0.2$) and weak positive correlations with HREE ($r = 0.5$) and host Fo content ($r = 0.4$).

5. Discussion

We have shown above that the 1669 melts, trapped in olivine, exhibit a linear mixing array of compositions, with one end-member enriched in LREE (and Zr and Nb), depleted (relative to similarly compatible elements) in Sr and containing low concentrations of S and CO₂ (Figures 5 and 6 and S3 and S4). The other end-member melt is depleted in LREE, and relatively enriched in Sr, CO₂, and S. Fractionation of pyroxene is not capable of generating the range in, for example, Ce/Y observed in the melt inclusions (Figures 5a and 5b); the range in Ce/Y (and in other LREE/HREE trace element ratios) must instead be inherited either from primary melts from the mantle or from modification of melts in the crust. Linear correlations between S and CO₂ in melt inclusions are not expected to result from degassing at Mt. Etna (Spilliaert, Allard, et al., 2006), or elsewhere (Métrich & Wallace, 2008) owing to the much lower solubility of CO₂ in silicate melts over sulfur (Witham et al., 2012). These trends instead indicate an intrinsic relationship between trace element ratios and volatile systematics generated by processes beyond simple fractional crystallization and degassing. We propose that this array was generated by mixing the two liquids in a shallow magma reservoir prior to eruption, where the mixing process was “captured” by the entrapment of melt inclusions. We discuss below why we believe that the LREE-depleted, Sr-, C-, and S-rich end-member may have ascended rapidly from depth, supersaturated. First, however, we consider how the relatively evolved 1669 end-members of the mixing array may have been generated by fractional crystallization of primitive melts beneath Mt. Etna (exemplified by the primitive FS tephra melts; Kamenetsky et al., 2007), then we discuss the possible origin of the LREE-depleted, Sr-, C-, and S-rich end-member in terms of mantle and crustal processes.

5.1. Modeling Fractional Crystallization of Two Geochemically Distinct Melts

The primitive melt observed as melt inclusions from the FS eruption (Kamenetsky et al., 2007) was used as a starting composition to model fractional crystallization (using Petrolog3; Danyushevsky & Plechov, 2011) at NNO+1 (Métrich & Clocchiatti, 1996), 1100 °C (Kamenetsky & Clocchiatti, 1996), and for two pressures: 100 MPa (Kahl et al., 2017) and 400 MPa (Kamenetsky et al., 2007), which might be suitable for FS melt fractionation. We use examples of enriched and depleted (as indicated by Ce/Y) FS melt inclusions as a starting point for the modeling because (a) the FS melt inclusions are the most primitive to be observed at Mt. Etna, at ~13 wt% MgO (other primitive whole rocks have < 9 wt% MgO; Corsaro & Métrich, 2016) and (b) the FS melt inclusions exhibit a similar range in Ce/Y to the 1669 melt inclusions, which is independent of fractional crystallization and (c) a full set of compositional data (volatiles and major and trace elements) is available for the FS melt inclusions. We recognize, however, that previous studies have identified that the FS tephra has anomalously high CaO compared to other Mt. Etna magma compositions, as well as high radiogenic Sr and Rb/Th, which has been ascribed to a high degree of melting of a mantle source with considerable pyroxenite component (Corsaro & Métrich, 2016).

Fractional crystallization trends from Petrolog (Danyushevsky & Plechov, 2011) at 100 and 400 MPa are marked onto Figure 3 using the most depleted and enriched end-member FS melts as a starting point for each pressure. The melts erupted during the CE 1669 and other recent eruptions have undergone fractionation of augite, as shown by the inflection point on the liquid line of descent at 9 wt.% MgO where CaO begins to be depleted in the melt (Figure 3). Plagioclase crystallization begins at ~4 wt.% MgO, shown by depletion in both Al₂O₃ and CaO together (Figure 3). The fractional crystallization models, where the order of crystallization is olivine→olivine+augite→olivine+augite+plagioclase, describes well the Al₂O₃ and CaO contents of the melts, although cannot reproduce the observed K₂O and Na₂O concentrations, which are higher than

predicted from the models (Figures 3b and 3d). This may be a consequence of the relatively low alkali content of the FS melts compared to other magma compositions from Mt. Etna, as identified previously (Corsaro & Métrich, 2016). However, the models describe the evolution of the trace element concentrations well. We find that 70% fractional crystallization at 1 kbar of the least LREE-enriched FS melt (melts with the lowest Ce/Y; Figure 5a; Kamenetsky et al., 2007) yields a melt with the same LREE/HREE ratio as the least enriched melts in the CE 1669 melt inclusions (Ce/Y 2-3), with a similar absolute concentration of trace elements (Figure 5a). In the same way, 70% fractional crystallization of the most LREE-enriched FS melt (with Ce/Y 6) yields the observed LREE absolute concentrations of the enriched melts (with Ce/Y 6) of the CE 1669 inclusion suite.

We propose that the array of evolved compositions in the CE 1669 melt inclusions requires up to 70% fractionation of two primitive melt compositions that have similar end-member trace element compositions to the FS melt but may be more alkali-rich. The LREE-depleted and LREE-enriched melts mix (to produce the observed melt inclusion array) only after each has undergone significant differentiation, thus yielding the observed high trace element compositions and the array in LREE/HREE observed in the 1669 MI suite (Ce/Y: 2-6, Nb 50-140, and La 60-140; Figures 4 and 5). Mixing and fractionation was not concurrent because (a) the trace element array seen in the 1669 melt inclusions is associated with a limited range in the MI major elements and is not systematic with the evolution of the olivine Fo mol.% and (b) melt inclusions within a single olivine crystal can have the full range of enrichment and absolute trace element concentration observed in the entire data set (Figure S2). We have therefore established that the two end-member melts that mixed to form the 1669 compositional array could feasibly have formed from the fractional crystallization of liquids similar to the two extreme compositions sampled by the melt inclusions in the primitive FS tephra (Kamenetsky et al., 2007). But what then is the origin of the LREE, Sr and volatile systematics of the two end-member melts? Did these melts acquire their geochemical features in the mantle or in the crust?

5.2. Sr-Enrichment in 1669 Depleted Melts

Principal component analysis of the 1669 melt inclusion trace element compositions indicates that the first two principal components describe 50% of the variance in trace element data set (see the supporting information). The first principal component (PC1) highlights an anomaly in the behavior of Sr, caused by a process that is fractionating Sr from other elements (Figure S5). PC1 may be due to addition or removal of plagioclase (Sr is compatible in plagioclase, while all other REEs are incompatible and become enriched in the melt) or assimilation of Sr from some source or contaminant, and this may also affect the different PC1 scores of HREE compared to LREE. PC2 is positive for the LREE and negative for the HREE (Figure S5) and might therefore be related to (1) the depth of melting and the presence of garnet in the melting region where HREE are compatible; (2) the degree of mantle melting, which affects the degree of LREE enrichment; or (3) the trace element composition of the mantle source. The process controlling PC2 is responsible for the observed range in LREE/HREE of the end-member melts. Sr, however, does not behave like the LREE as expected (Figures 4c and S3). Sr has a negative PC2 like the HREE, and this is likely to be due to the combined effect of the strontium anomaly with nonorthogonal mantle and crustal processes (Figure S5). The principal component analysis approach has not managed to clearly separate out the processes here. The crucial difference between PC1 and PC2 is in the behavior of the MREEs (Figure S5), and this is important for understanding the controlling processes.

The abundance of Sr in both the primitive FS melts and the 1669 LREE-depleted melts is anomalous, as Sr is enriched with respect to its compatibility compared to other REE, that is, Sr/Sr* (Figures 5 and S4). There is a strong negative correlation between Sr/Sr* in the melt inclusions and LREE (La and Ce), Ba, Nb, and Zr ($r = -0.82$ to -0.71); and a strong positive correlation between Sr/Sr* and CaO, CO₂, and S ($r = 0.57$ to 0.67 ; Figure S3). In the case of the FS melts, these correlations cannot be explained using olivine fractional crystallization alone (or the postentrapment crystallization of olivine on the melt inclusion walls) since this should affect elements with neighboring compatibility (Sr, Ce, and Nd) in a similar way. A number of processes that affect Sr enrichment in the FS primitive melts and the more evolved 1669 melts are considered here.

Sr enrichment in melt inclusions may be caused by (1) involvement of a Sr-rich mantle source component either from pyroxenite (Correale et al., 2012) or a “ghost plagioclase” signature inherited from an eclogitic component in the mantle source (Sobolev et al., 2000); (2) plagioclase assimilation within the crust by primitive melts (Danyushevsky et al., 2003), in which LREE are highly incompatible; (3) accumulation of small

fraction lower crustal gabbroic melts (Annen et al., 2005); and (4) assimilation of crustal carbonate over a range of pressure and temperature (Carter & Dasgupta, 2015; Marziano et al., 2008; Michaud, 1995). The two potential sources of Sr, one from the mantle (eclogitic oceanic crust and/or a pyroxenite source) and one from the crust (plagioclase, gabbroic cumulates, or carbonates), would have quite different implications for the volatiles, in particular the flux of volcanic carbon, as (a) the solubility of volatiles in silicate melts is dependent on the major element composition of the melt (Moore, 2008) and (b) because some of these mechanisms involve volatile-rich sources (e.g., crustal carbonate and/or recycled lithologies). We discuss each of these mechanisms in turn.

5.2.1. Mantle Source Heterogeneity as the Source of the Sr Anomaly

Trace element and Sr isotope data for dyke-fed eruptions have revealed that mantle source heterogeneities, and particularly the variable involvement of a clinopyroxenitic lithology, have a strong influence over the degree of melting of the heterogeneous mantle and long-term magmatic processes beneath Mt. Etna (Corsaro & Métrich, 2016). The Sr anomaly in the primitive melts could therefore be inherited from the mantle due to incorporation of (i) small fractions of pyroxenite melt (Correale et al., 2012; Correale et al., 2014) or (ii) melts of recycled lower oceanic crustal plagioclase-bearing cumulates in the melting region. In the mantle melting region under Mt. Etna the restite of these recycled materials will be plagioclase free (e.g., eclogite), with a low bulk partition coefficient for Sr. Melts derived from recycled cumulates may therefore inherit the positive Sr/Sr anomaly of their sources (Sobolev et al., 2000).

We explore the possible mantle origins of compositional variation in the melt inclusion suite by modeling incremental fractional melting of KLB-1 peridotite (Davis et al., 2009; Jennings & Holland, 2015) and KG1(8) pyroxenite (Jennings et al., 2016; Kogiso et al., 1998) at 1315 and 1500 °C after Jennings and Holland (2015) and Jennings et al. (2016), respectively, using pressure-temperature-melt fraction pathways for decompression melting calculated assuming anhydrous and isentropic conditions according to (Katz et al., 2003; further details are given in the supporting information). Instantaneous 0.01 melt fractions were generated by the model and accumulated to obtain the trace element composition of melt fractions from 0 to 0.2. There are numerous solutions that can generate the FS melt end-member LREE/HREE ratios using a combination of the degree of melting of both sources and the degree of mixing between them (Figure 7a). A 10% pyroxenite, 90% peridotite composition has been proposed previously for FS melts using mantle xenoliths (Correale et al., 2012), but our modeling suggests that this solution is non-unique given the degrees of freedom in a combination of melt fraction and proportions of mixing sources. A more concrete result of the modeling is that there is no solution that gives a melt with both Sr enrichment and LREE-depletion (Figure 7).

An eclogite melting signature (associated with melting of recycled gabbroic cumulates) was proposed to explain the geochemistry of melt inclusions in olivines from Mauna Loa, Hawaii (Sobolev et al., 2000). Sr-rich melts from Mauna Loa show depletion in incompatible elements, including negative Nb and Zr anomalies (Sobolev et al., 2000). This distinctive trace element signature may be inherited from *plagioclase*, as is commonly observed in ophiolitic cumulates. It is proposed that gabbro may retain its chemical identity throughout convective cycling in the mantle without mixing with other parts of the subducted oceanic crustal sequence, yielding a “ghost plagioclase” signature and Sr anomalies in the resulting ocean island melts. Melting models for different mantle sources show that eclogite melts are very small in volume and are readily lost in the bulk magma, but even a small fraction of eclogite-derived melts can have a significant effect on the REE chemistry. A mixture of 90% peridotite melt and 10% eclogite-derived melt provide a possible explanation for the observed REE and major element chemistry seen at Mauna Loa (Sobolev et al., 2000). The same geochemical anomalies as observed in the Mauna Loa melt inclusions (Sobolev et al., 2000) are observed in the Sr-rich, LREE-depleted FS, and 1669 melts (Figure 5), making melting of recycled gabbroic cumulates in the mantle source region a plausible explanation for the presence of such anomalies.

5.2.2. Resorption of Plagioclase as the Source of the Sr Anomaly

Early-formed plagioclase crystals trapped in MI can react with the host olivine and melt at high magmatic temperatures, resulting in a Sr-enriched melt composition (Danyushevsky et al., 2003; Schiavi et al., 2015; Figure 7b). Plagioclase assimilation by complete dissolution was modeled using a plagioclase composition from a Mt. Etna eruption (Viccaro et al., 2006) that was similar in composition to the 1669 eruption (Corsaro et al., 1996). The blue line in Figure 7b shows that up to 30% plagioclase dissolution is required to be mixed with the FS depleted end-member to give a melt composition that, after fractional

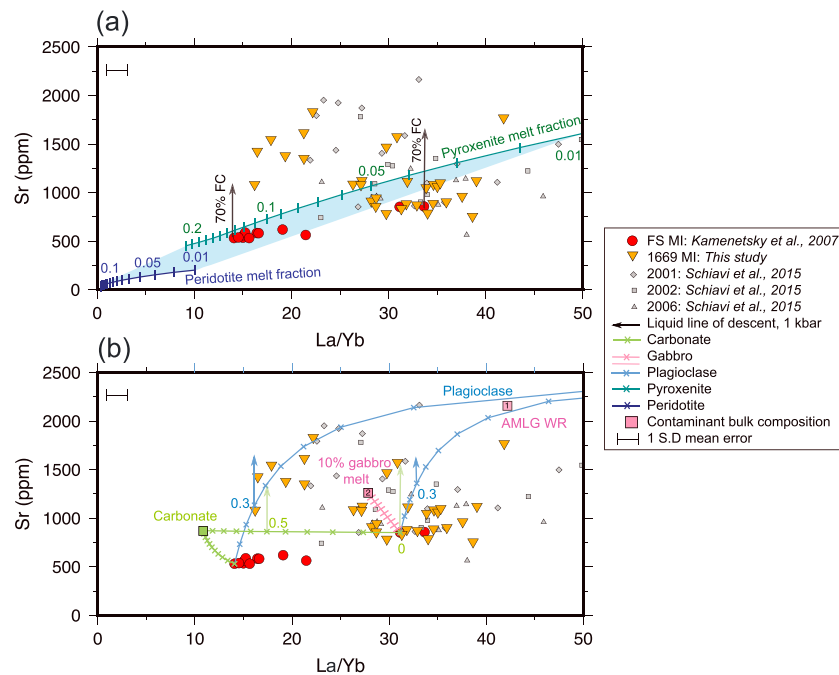


Figure 7. Model of possible mechanisms to account for Sr-rich, CO₂-rich depleted melts mixing with Sr-poor, CO₂-poor, enriched melts in the shallow crust. MI symbols for 1669, Fall-Stratified (FS) and 2001, 2002, and 2006 same as before. Fractional crystallization (FC) of FS-melt modeled by Petrolog3 software (Danyushevsky & Plechov, 2011) indicated by vertical arrows. (a) Model of mantle melting: (i) KG1(8) pyroxenite melting at F=0.01 accumulated fractions (turquoise), ticks mark degree of melting. (ii) KLB-1 peridotite melting at F=0.01 accumulated fractions (dark blue line), ticks mark degree of melting. (b) Models of contaminant assimilation: (i) plagioclase (blue line) assimilation: ticks mark fraction of contaminant mixed into depleted and enriched FS-melts, and blue arrows signify 70% FC of the end-member melts after 30% contamination by plagioclase; (ii) 10% gabbro melt (pink line) assimilation: ticks mark fraction of contaminant mixed into enriched FS-melts. The pink box 1 is the whole rock (WR) composition of the AMLG gabbro (Corsaro et al., 2014), and the box 2 is the composition of the 10% batch melt from this gabbro (iii) carbonate (green line) assimilation; ticks mark fraction of contaminant mixed into LREE-enriched and LREE-depleted FS-melt. The green box is the composition of Etnean carbonate xenolith contaminant. The green arrows signify 70% FC of the LREE-enriched melt after 0% carbonate assimilation (i), and 50% carbonate assimilation (ii).

crystallization, will have a high enough Sr concentration to match the LREE-depleted 1669 melts. However, complete dissolution is not realistic and plagioclase reacts incongruently in the melt inclusion according to plagioclase + melt + host olivine → spinel + olivine + melt (Danyushevsky et al., 2003). Overall, the vector describing the progressive assimilation of plagioclase is inconsistent with the trends seen in the 1669 major and trace element data (vectors; Figure 3 and 7).

5.2.3. Lower Crustal Gabbro Assimilation as the Source of the Sr Anomaly

Localized remelting of lower crustal gabbroic material is possible by fluid-rich, metasomatized mantle melts with a more primitive bulk composition to the lower crust (Annen et al., 2005; Figure 7b). Assimilation of gabbro was modeled for the Etnean AMLG gabbro (enclosed in 2001 lavas), with the highest whole rock Sr (Corsaro et al., 2014; pink box 1; Figure 7b). Melting of this gabbro (10%) was modeled using a batch melting equation (see equation (1) in the supporting information) and mixed with the enriched end-member of the FS melt to determine whether gabbroic assimilation could yield the positive Sr anomaly (and LREE depletion) described by the 1669 melts (pink line, pink box 2 indicates 10% melted gabbro composition, Figure 7b). Addition of gabbroic melts, even with 100% mixing, did not give comparable Sr concentrations, primarily because the bulk solid-melt partition coefficient for Sr is too high. Nor did the REE become fractionated enough to reduce the LREE/HREE ratio and give a more depleted melt signature, comparable to the 1669 depleted MI. Additionally, progressive assimilation of gabbro does not follow the major element oxide trends seen in 1669 MI (Figure 3). We therefore reject remelting of gabbro as a mechanism to generate the observed Sr anomaly and LREE depletion observed in the FS and 1669 melt inclusions.

5.2.4. Magmatic Assimilation of Crustal Carbonate and/or Associated Fluids

A potential source of Sr is carbonate melt or fluid assimilation during transport and storage of melts in the 40-km-thick Etnean crust. The whole rock Sr isotope composition of the 1669 lavas ranges from 0.70330 to 0.70344 and are very similar to MORB (Corsaro et al., 1996). This low radiogenic Sr isotopic composition does not preclude assimilation of Sr from Cretaceous carbonates, however, which have Sr isotope composition of 0.707 and are significantly less radiogenic than the continental crust (mean 0.716; Elderfield, 1986).

Carbonate assimilation is modeled using a carbonate composition derived from a xenolith found in 1982 lava (Corsaro et al., 2014). Addition of carbonate to the FS LREE-enriched end-member (green line, Figure 7b) yields a higher Sr concentration in the melt but reduces the LREE concentration, giving a more depleted LREE/HREE, but Sr-enriched melt. Melt compositions generated by 40-50% assimilation of carbonate into the enriched melt and up to 70% fractional crystallization are very similar to the LREE-depleted and Sr-rich end-member melt of the 1669 eruption (Figure 7). The carbonate assimilation here is the maximum possible since it is assumed here that an enriched-FS end-member melt is the parental melt, when in fact the depleted 1669 melt inclusions may have been sourced from a more depleted primitive melt. It is possible that both parental melts have undergone some carbonate assimilation before mixing and by different amounts, with the more depleted parental melt assimilating more carbonate so as to result in a greater Sr anomaly than the enriched melt.

However, assimilation of these high percentages of carbonate material is unrealistic when we consider their potential effect on major element oxides (Figure 3). Assimilation of carbonate causes an increase in the CaO content of the melt (vectors: Figure 3c) and increased clinopyroxene (cpx) nucleation and crystallization with compositional progression toward Ca-Tschermak cpx (Mollo et al., 2010). This depletes the melt in MgO and SiO₂, consumes olivine and plagioclase, and crystallizes scapolite and spinel, thus changing the modal proportions of phases in the system (Carter & Dasgupta, 2015; Marziano et al., 2008; Mollo et al., 2010). The model results in an enrichment of alkalis in the melt (Figures 3b and 3d) as these are not compatible in cpx. The degree of assimilation, the resulting phase assemblage and melt composition, and the CO₂ fluid release is PT dependent, with LP and HT conditions having the greatest assimilation potential. Experiments show that at 0.5 GPa 21-48% carbonate can be assimilated between 1100 and 1200 °C and the CO₂ fluid produced at 1 GPa between 1100 and 1175 °C increases from 0.09 to 0.28 g per gram of basaltic melt (Carter & Dasgupta, 2015). The CO₂-rich fluid phase causes dehydration of the melt and increases the CO₂/H₂O ratio of the free fluid phase. The enhanced CO₂ fugacity in the fluid phase and the increased melt CaO content may increase the solubility of CO₂ in the melt. The composition of the C—O—H fluid affects the redox state of the carbonated system, and experiments by Mollo et al. (2010) show that *f*O is lowered by two log units when a CO₂-rich C—O—H fluid is present. However, fluid migration away from the reservoir may cause the opposite effect.

The extent of carbonate assimilation is limited by the MgO content of the system (Carter & Dasgupta, 2015). Melts at Vesuvius are phonolitic in composition due to a reduction in MgO and enrichment in alkalis and show evidence for carbonate assimilation (Carter & Dasgupta, 2015; Freda et al., 2008). Progressively more carbonate assimilation leads to alkali-rich, MgO-poor and SiO₂-poor melts that are foititic in composition, such as those from the Colli Albani Volcanic District (Freda et al., 2008; Gaeta et al., 2009). Oxygen isotopes support carbonate assimilation by these magmas, as well as the presence of skarns and the high CO₂ flux from Italian volcanic systems (Chiodini et al., 2004). For Mt. Etna it has been estimated that 41-92% of magma (the experiments used a synthetic K-basalt) would need to react with calcite to explain the observed emission rate of CO₂ (Carter & Dasgupta, 2015). The 1669 melts, however, are not ultracalcic and silica-poor as would be expected from the percentage of carbonate required to yield the Sr anomaly (Figure 7). However, the depleted 1669 melts do show a higher CaO content (Figure 3c) than the enriched melts.

5.3. The Implications of Melt Heterogeneity for Volatile Systematics

The negative correlation between CO₂ and Nb ($r = -0.68$; Figures 6c and S3) contrasts with the positive correlation measured in vapor-undersaturated melt inclusions from the Siqueiros fracture zone on the East Pacific Rise (Saal et al., 2002) and calculated for undegassed Mid-Atlantic Ridge basalts (Cartigny et al., 2008). Other CO₂-trace element data sets in the literature either record significant variability in CO₂ with

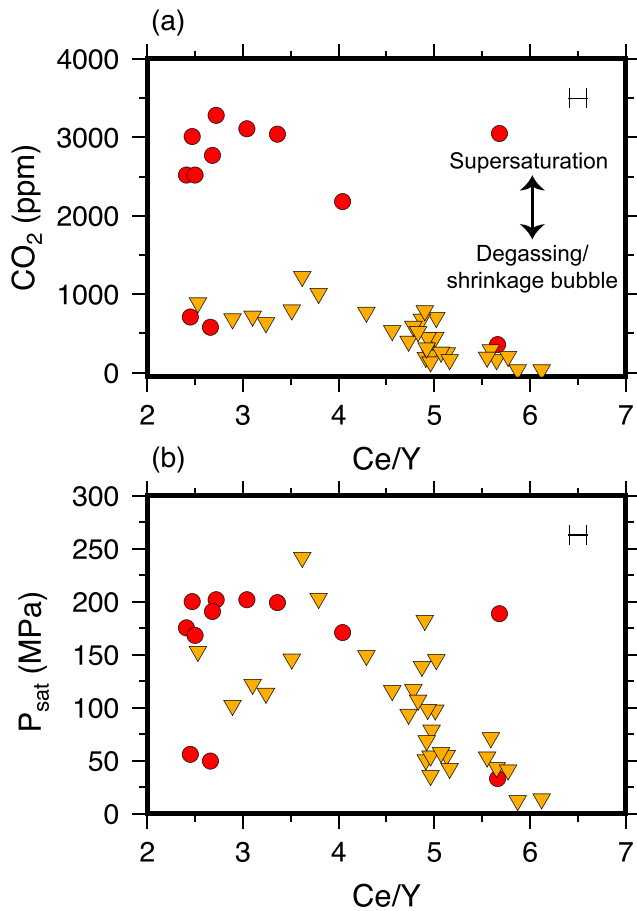


Figure 8. (a) Melt inclusion CO₂ concentrations plotted against Ce/Y for both 1669 melts (orange triangles) and Fall-Stratified (FS) melts (red circles). (b) Saturation pressures calculated using major element parameterization (Shishkina et al., 2014), which takes into the account the variable CaO and alkali contents of the end-member melts, plotted against Ce/Y.

near-constant Nb (Shaw et al., 2010) or show no robust correlations between the two species (Dixon & Clague, 2001; Helo et al., 2011; Koleszar et al., 2009; Workman et al., 2006). Melt inclusions are usually partly degassed with respect to CO₂, and this lack of correlation commonly reflects this. A negative correlation between CO₂ and incompatible trace elements was observed in a melt inclusion suite from Skuggafjöll, Iceland (Neave et al., 2014), and could arise during olivine cooling, PEC, and the formation of a shrinkage bubble. However, the low degree of PEC (5-10%; Table S5) observed in the 1669 melt inclusions and analysis of shrinkage-bubble-free MI means that the full range in incompatible element concentrations is not reproducible with this mechanism. Modeling of mid-ocean ridge volatile systematics has shown that this negative correlation may also arise during concurrent mixing and degassing at a range of pressures (Matthews et al., 2017), although this mechanism cannot reproduce the CO₂-Sr-REE systematic we observe for the 1669 melt inclusions.

We propose that the positive correlation between Sr and CO₂ ($r = 0.63$) and between Sr/Sr* ($r = 0.67$) observed in the melt inclusion suite represents a mixing signature, as discussed above. In order for two equilibrium melts, with different CO₂ concentrations, to mix at the same pressure requires the solubility of CO₂ in the two melts to be different (Dixon, 1997; Shishkina et al., 2014). The depleted and enriched melts observed in both the 1669 and FS melt inclusion suites (one with low LREE and high Sr, the other with high LREE and low Sr) have different major element oxide compositions, with up to 2 wt.% differences in CaO, KO, NaO, and AlO (Figure 3). These differences are sufficient to cause differences in CO₂ solubility. Melts that are rich in calcium (Ca) and alkalis (K and Na) stabilize higher concentrations of CO₂ (Moore, 2008; Shishkina et al., 2014). Sulfur fluid-melt partitioning is also reduced as the mole fraction of Ca and Al in the melt increases (Zajacz, 2015) leading to the melt being able to dissolve more sulfur (in the absence of sulfide or sulfate saturation). Differences in major element composition between the two end-member melts may explain the strong correlation between

CO₂ and S ($r = 0.73$), and the negative correlations between CO₂ and LREE ($r = -0.68$ to -0.59) and positive correlations between CO₂ and Sr ($r = 0.63$), which are not consistent with degassing trends. A degassing trend would deplete CO₂ at greater pressures than S, resulting in an array of shallow-trapped melts with low CO₂ and variable sulfur. For a degassing trend alone, correlations between CO₂ and S and LREE and Sr would not be expected. For CO₂ fluxing and degassing-induced crystallization (Cashman & Blundy, 2000), trends of increasing CO₂, decreasing S, and increasing LREE would be expected, which are not observed (Figure 6).

The major element parameterization of CO₂ solubility (Shishkina et al., 2014; Figure 8) yields equilibrium pressures of ~200 MPa for the high-CO₂ FS melt inclusions, rather than 400 MPa using VolatileCalc (Kamenetsky et al., 2007; Newman & Lowenstern, 2002) because these melts are rich in Ca and alkali elements, which enhances the solubility of CO₂. The different solubilities for the depleted and enriched FS melts (red circles, low and high Ce/Y; Figure 8a), caused by their different CaO and alkali contents, provide a mechanism for CO₂-rich and CO₂-poor melts to mix at the same pressure, at ~200 MPa (Figure 8b), rather than over the range 380-500 MPa as predicted by a solubility model that does not include compositional dependence (Kamenetsky et al., 2007). It is important to note, however, that the FS melt inclusions contain shrinkage bubbles, which may have sequestered some CO₂ (there are three FS melt inclusions with CO₂ < 1,000 ppm; Kamenetsky et al., 2007); hence, the actual trapping pressure was likely higher. For the 1669 melt inclusions (orange triangles; Figure 8), those with the highest CO₂ (>500 ppm) are the most depleted in their LREE contents (Ce/Y < 4) and are also richer in Ca and Mg but poorer in alkalis (Figure 3), which yields a

mean equilibration pressure of ~150 MPa (Figure 8b), although there is considerable scatter (Shishkina et al., 2014). However, the differences in major element composition and CO₂ solubility for the 1669 melt inclusions cannot entirely reconcile their saturation pressures (Figure 8b), with the more enriched melts (Ce/Y > 4) exhibiting a large range (20-180 MPa) and a lower mean (70 MPa) equilibration pressure than the depleted melts (with Ce/Y < 4; Figure 8b). If the melt inclusions were all entrapped together, in one shallow storage region, one might expect them all to record similar equilibration pressures, yet this is clearly not the case.

Another possibility to explain the observed range in “apparent” pressures for the mixing array (orange triangles, Figure 8b) is that the depleted end-member melt may be supersaturated with respect to carbon and sulfur upon mixing. Supersaturation may develop when basalts ascend from magma reservoirs to the surface faster than CO₂ can diffuse into bubbles, for example, as proposed for the Skuggafjöll melt in the Eastern Volcanic Zone of Iceland (Neave et al., 2014), or in submarine basaltic glasses where CO₂ concentrations often exceed the equilibrium concentrations predicted from solubility models (Dixon et al., 1988; Helo et al., 2011; Soule et al., 2012). Experiments were carried out to investigate the vesiculation of basalts from Stromboli (Pichavant et al., 2013). Natural pumice and glass samples were used to simulate melt ascent from 2-2.5 kbar to 0.25-0.5 kbar, and it was found that at a decompression rate equivalent to an ascent rate of 0.25 to 1.5 m/s, CO₂ concentrations were up to an order of magnitude higher than the solubility at the final pressure, corresponding to supersaturation pressures of ~150 MPa. At low vesicularity and/or bubble number density, CO₂ exsolution was limited by the rate of CO₂ diffusion through the melt, rather than the rate of CO₂ transfer across melt/vesicle interfaces, resulting in disequilibrium degassing (similar to rhyolite studies; Mangan & Sisson, 2000). The composition used by Pichavant et al. (2013) is slightly more hydrous (2.7-3.8 wt.%) than the 1669 Mt. Etna samples (1.4 wt.%), but the CO₂ content is very similar (up to 1,200 ppm). The ascent timescales for the melt to become CO₂ supersaturated upon arrival into a shallow magma reservoir is on the order of hours to days, depending on the vesicle number (Neave et al., 2014), which is comparable to the ascent times from reservoir depths estimated for Etnean eruptions of a few hours (from seismicity during the explosive flank eruption in 2002 at Mt. Etna; Patanè et al., 2003), or a few days (from the CE 1669 contemporary records of vigorous seismic events preceding the CE 1669 eruption by 2 weeks and focused at the eventual site of the Monti Rossi cone; Mulas et al., 2016; Tanguy et al., 1996, and references therein). Sulfur is strongly positively correlated with CO₂ ($r = 0.73$; Figure S3), suggesting that the depleted melt may also be supersaturated in sulfur upon mixing, consistent with the similar diffusivities of CO₂ and S in basaltic melts (Baker et al., 2005; Freda et al., 2005).

6. Implications and Comparison with Previous Work

Melt inclusions hosted by olivines erupted during the initial stages of the 1669 eruption of Mt. Etna, Italy, preserve a record of melt mixing. Two relatively evolved basaltic melts (each had undergone ~70% fractional crystallization) mixed to form an array of compositions with one end-member (perhaps slightly more primitive) depleted in LREE, enriched in Sr, Ca, carbon, and sulfur intruding a shallow storage region containing a melt relatively enriched in LREE, and relatively depleted in Sr, carbon, and sulfur. We propose that the LREE-depleted melt, which was rich in Sr, may have been generated by either the incorporation of a melt derived from a Sr-enriched recycled cumulate gabbro in the mantle or by incorporation of crustal carbonate. In either case, the modification in major element (Ca, Na, and K, in particular) composition of the melt caused the solubility of carbon and sulfur in the melt to increase. Rapid rise of such depleted, volatile-rich melts may have caused the melt to become supersaturated, such that upon arrival into the shallow plumbing system, where the melts stalled and mixed with resident melts, a vigorous episode of degassing would have taken place, both in response to rapid equilibration and in response to cooling upon mingling with the stored melts. This cooling would have caused a burst of crystal growth, allowing melt inclusions to be trapped which recorded the mingling and mixing of these two distinct melts.

Magma mixing prior to and during the 1669 eruption of Mt. Etna is consistent with previous work. Corsaro et al. (1996) identified two lava types based on their geochemistry: SET1 and SET2. SET1 was erupted during 11-20 March 1669 and were more primitive than the later-erupted SET2. The lava types were interpreted as having coexisted and interacted in the magmatic storage system prior to eruption, with the lower density, volatile-rich SET1 magma rising up through the SET2 magma. Kahl et al. (2017) deduced additional detail

from study of olivine core and rim compositions, combined with timescales from diffusion modeling. SET1 magmas contained olivines with core compositions similar (Fo_{75-78}) to those we analyze in this study (Fo_{74-75} ; Kahl et al., 2017). The magma was invaded by a more evolved melt 1–2 years prior to eruption, which gave rise to the lower forsterite rims, which continued up to a few weeks or months prior to eruption (Kahl et al., 2017). The intruding melts ascending rapidly up to shallow levels in the system may have carried high fractions of exsolved (and dissolved) volatiles.

Mixing between supersaturated melts (with their bulk CO_2 content enhanced by due to their Ca- and alkali-rich composition) and stored, degassed melts shortly before eruption may explain observations of enhanced CO_2 fluxes prior to eruptions at Mt. Etna (Aiuppa et al., 2007; Aiuppa et al., 2008). Mixing of magmas with markedly different compositions (mafic injected into more evolved magmas) has been proposed as a means to trigger eruptions at many stratovolcanoes (Venezky & Rutherford, 1997; Woods & Cardoso, 1997), but in the case of 1669 and recent eruptions at Mt. Etna (Ferlito et al., 2010; Métrich et al., 2004; Viccaro et al., 2006), both mixing magmas have a basaltic composition. The critical factors controlling eruption triggering may be the differential volatile contents and solubility in the melt due to differences in major element composition. Evidence is presented that indicates that incompatible element-depleted melts may ascend rapidly through the midcrust and upper crust beneath Mt. Etna, developing supersaturation in the volatiles carbon dioxide and sulfur and thereby suppressing their outgassing into a vapor phase. The arrival of these melts into shallow magma storage areas may prompt rapid cooling and vesiculation, the conditions necessary to trap melt inclusions (during rapid crystal growth) and to trigger eruptions (through vesiculation and increase in overpressures). This process of intrusion of volatile-charged, supersaturated melts may be a common process not only at Mt. Etna but also at many other basaltic volcanoes worldwide. This study further supports the growing assertion that melt inclusion arrays of H_2O , and CO_2 compositions only very rarely show degassing pathways; more commonly, the diffuse array of data reflects composition-dependent solubility, disequilibrium (supersaturation in CO_2 over H_2O), and mixing.

Acknowledgments

This work was supported by a Natural Environment Research Council studentship to L. C. Salem (NE/L501578/1) and a Natural Environment Research Council Ion Microprobe Facility award (IMF483/0513). We thank Robin Clarke, Martin Walker, and Iris Buisman for help with sample preparation and EPMA at the University of Cambridge. We thank all the staff, and Richard Hinton in particular, for their assistance with SIMS analyses at the Ion Microprobe Facility at University of Edinburgh. We thank David Neave for helpful discussions. We acknowledge insightful reviews from Nicole Métrich, Kayla Iacovino, Terry Plank, Eniko Bali, and one anonymous reviewer, which improved this manuscript enormously. We thank Associate Editor Tobias Fischer and Editor Claudio Faccenna for their handling of this manuscript. All the data used are listed in the references or contained within the supporting information.

References

- Aiuppa, A., Federico, C., Giudice, G., Gurrieri, S., Liuzzo, M., Shinohara, H., et al. (2006). Rates of carbon dioxide plume degassing from Mount Etna volcano. *Journal of Geophysical Research*, *111*, B09207. <https://doi.org/10.1029/2006JB004307>
- Aiuppa, A., Giudice, G., Gurrieri, S., Liuzzo, M., Burton, M., Caltabiano, T., et al. (2008). Total volatile flux from Mount Etna. *Geophysical Research Letters*, *35*, L24302. <https://doi.org/10.1029/2008GL035871>
- Aiuppa, A., Moretti, R., Federico, C., Giudice, G., Gurrieri, S., Liuzzo, M., et al. (2007). Forecasting Etna eruptions by real-time observation of volcanic gas composition. *Geology*, *35*(12), 1115–1118. <https://doi.org/10.1130/G24149A.1>
- Allard, P., Behncke, B., D'Amico, S., Neri, M., & Gambino, S. (2006). Mount Etna 1993–2005: anatomy of an evolving eruptive cycle. *Earth-Science Reviews*, *78*(1–2), 85–114. <https://doi.org/10.1016/j.earscirev.2006.04.002>
- Allard, P., Carbone, J., Dajčević, D., Le Bronec, J., Morel, P., Robe, M., et al. (1991). Eruptive and diffuse emissions of CO_2 from Mount Etna. *Nature*, *351*(6325), 387–391. <https://doi.org/10.1038/351387a0>
- Aloisi, M., Cocina, O., Neri, G., Orecchio, B., & Privitera, E. (2002). Seismic tomography of the crust underneath the Etna volcano, Sicily. *Physics of the Earth and Planetary Interiors*, *134*(3–4), 139–155. [https://doi.org/10.1016/S0031-9201\(02\)00153-X](https://doi.org/10.1016/S0031-9201(02)00153-X)
- Andronico, D., Branca, S., Calvari, S., Burton, M., Caltabiano, T., Corsaro, R. A., et al. (2005). A multi-disciplinary study of the 2002–03 Etna eruption: Insights into a complex plumbing system. *Bulletin of Volcanology*, *67*(4), 314–330. <https://doi.org/10.1007/s00445-004-0372-8>
- Andronico, D., & Corsaro, R. (2011). Lava fountains during the episodic eruption of South–East Crater (Mt. Etna), 2000: Insights into magma-gas dynamics within the shallow volcano plumbing system. *Bulletin of Volcanology*, *73*(9), 1165–1178. <https://doi.org/10.1007/s00445-011-0467-y>
- Annen, C., Blundy, J., & Sparks, R. (2005). The genesis of intermediate and silicic magmas in deep crustal hot zones. *Journal of Petrology*, *47*(3), 505–539.
- Baker, D. R., Freda, C., Brooker, R. A., & Scarlato, P. (2005). Volatile diffusion in silicate melts and its effects on melt inclusions. *Annals of Geophysics*, *48*, 4–5.
- Bottari, A., Broccio, F., & Giudice, E. O. (1975). Some seismological results and geostructural suggestions from a study of the Reggio Calabria earthquake of 16 January, 1975. *Annals of Geophysics*, *28*(2–3), 219–239.
- Branca, S., De Beni, E., & Proietti, C. (2013). The large and destructive 1669 AD eruption at Etna volcano: reconstruction of the lava flow field evolution and effusion rate trend. *Bulletin of Volcanology*, *75*(2), 694. <https://doi.org/10.1007/s00445-013-0694-5>
- Branca, S., & Ferrara, V. (2013). The morphostructural setting of Mount Etna sedimentary basement (Italy): Implications for the geometry and volume of the volcano and its flank instability. *Tectonophysics*, *586*, 46–64. <https://doi.org/10.1016/j.tecto.2012.11.011>
- Branca, S., & Vigliotti, L. (2015). Finding of an historical document describing an eruption in the NW flank of Etna in July 1643 AD: timing, location and volcanic products. *Bulletin of Volcanology*, *77*(11), 95. <https://doi.org/10.1007/s00445-015-0979-y>
- Bucholz, C. E., Gaetani, G. A., Behn, M. D., & Shimizu, N. (2013). Post-entrapment modification of volatiles and oxygen fugacity in olivine-hosted melt inclusions. *Earth and Planetary Science Letters*, *374*, 145–155. <https://doi.org/10.1016/j.epsl.2013.05.033>
- Burton, M. R., Sawyer, G. M., & Granieri, D. (2013). Deep carbon emissions from volcanoes. *Reviews in Mineralogy and Geochemistry*, *75*(1), 323–354. <https://doi.org/10.2138/rmg.2013.75.11>
- Carter, L. B., & Dasgupta, R. (2015). Hydrous basalt–limestone interaction at crustal conditions: Implications for generation of ultracalcic melts and outflux of CO_2 at volcanic arcs. *Earth and Planetary Science Letters*, *427*, 202–214. <https://doi.org/10.1016/j.epsl.2015.06.053>

- Cartigny, P., Pineau, F., Aubaud, C., & Javoy, M. (2008). Towards a consistent mantle carbon flux estimate: Insights from volatile systematics (H_2O/Ce , δD , and CO_2/Nb) in the North Atlantic mantle ($14^\circ N$ and $3-44^\circ N$). *Earth and Planetary Science Letters*, *265*(3), 672–685. <https://doi.org/10.1016/j.epsl.2007.11.011>
- Cashman, K., & Blundy, J. (2000). Degassing and crystallization of ascending andesite and dacite. *Philosophical Transactions of the Royal Society of London. Series A: Mathematical, Physical and Engineering Sciences*, *358*(1770), 1487–1513. <https://doi.org/10.1098/rsta.2000.0600>
- Catalano, S., Torrisi, S., & Ferlito, C. (2004). The relationship between Late Quaternary deformation and volcanism of Mt. Etna (eastern Sicily): new evidence from the sedimentary substratum in the Catania region. *Journal of Volcanology and Geothermal Research*, *132*(4), 311–334. [https://doi.org/10.1016/S0377-0273\(03\)00433-5](https://doi.org/10.1016/S0377-0273(03)00433-5)
- Chiodini, G., Caliro, S., Aiuppa, A., Avino, R., Granieri, D., Moretti, R., & Parello, F. (2011). First 13 C/12 C isotopic characterisation of volcanic plume CO₂. *Bulletin of Volcanology*, *73*(5), 531–542. <https://doi.org/10.1007/s00445-010-0423-2>
- Chiodini, G., Cardellini, C., Amato, A., Boschi, E., Caliro, S., Frondini, F., & Ventura, G. (2004). Carbon dioxide Earth degassing and seismogenesis in central and southern Italy. *Geophysical Research Letters*, *31*, L07615. <https://doi.org/10.1029/2004GL019480>
- Chiodini, G., Granieri, D., Avino, R., Caliro, S., Costa, A., Minopoli, C., & Vilaro, G. (2010). Non-volcanic CO₂ Earth degassing: Case of Mefite d'Ansanto (southern Apennines), Italy. *Geophysical Research Letters*, *37*, L11303. <https://doi.org/10.1029/2010GL042858>
- Clocchiatti, R., Joron, J.-L., & Treuil, M. (1988). The role of selective alkali contamination in the evolution of recent historic lavas of Mt. Etna. *Journal of Volcanology and Geothermal Research*, *34*(3-4), 241–249. [https://doi.org/10.1016/0377-0273\(88\)90036-4](https://doi.org/10.1016/0377-0273(88)90036-4)
- Clocchiatti, R., & Metrich, N. (1984). Témoignages de la contamination dans les produits des éruptions explosives des M. Silvestri (1892) et M. Rossi (1669) (Mt. Etna). *Bulletin Volcanologique*, *47*(4), 909–928. <https://doi.org/10.1007/BF01952351>
- Collins, S. J., Pyle, D. M., & MacLennan, J. (2009). Melt inclusions track pre-eruption storage and dehydration of magmas at Etna. *Geology*, *37*(6), 571–574. <https://doi.org/10.1130/G30040A.1>
- Condomines, M., Tanguy, J.-C., & Michaud, V. r. (1995). Magma dynamics at Mt Etna: constraints from U-Th-Ra-Pb radioactive disequilibrium and Sr isotopes in historical lavas. *Earth and Planetary Science Letters*, *132*(1-4), 25–41. [https://doi.org/10.1016/0012-821X\(95\)00052-E](https://doi.org/10.1016/0012-821X(95)00052-E)
- Correale, A., Martelli, M., Paonita, A., Rizzo, A., Brusca, L., & Scribano, V. (2012). New evidence of mantle heterogeneity beneath the Hyblean Plateau (southeast Sicily, Italy) as inferred from noble gases and geochemistry of ultramafic xenoliths. *Lithos*, *132*, 70–81.
- Correale, A., Paonita, A., Martelli, M., Rizzo, A., Rotolo, S. G., Corsaro, R. A., & Di Renzo, V. (2014). A two-component mantle source feeding Mt. Etna magmatism: Insights from the geochemistry of primitive magmas. *Lithos*, *184*, 243–258.
- Corsaro, R., Métrich, N., Allard, P., Andronico, D., Miraglia, L., & Fourmentraux, C. (2009). The 1974 flank eruption of Mount Etna: An archetype for deep dike-fed eruptions at basaltic volcanoes and a milestone in Etna's recent history. *Journal of Geophysical Research*, *114*, B07204. <https://doi.org/10.1029/2008JB006013>
- Corsaro, R. A., Cristofolini, R., & Patané, L. (1996). The 1669 eruption at Mount Etna: chronology, petrology and geochemistry, with inferences on the magma sources and ascent mechanisms. *Bulletin of Volcanology*, *58*(5), 348–358. <https://doi.org/10.1007/s004450050144>
- Corsaro, R. A., & Métrich, N. (2016). Chemical heterogeneity of Mt. Etna magmas in the last 15 ka. Inferences on their mantle sources. *Lithos*, *252*, 123–134.
- Corsaro, R. A., Miraglia, L., & Pompilio, M. (2007). Petrologic evidence of a complex plumbing system feeding the July–August 2001 eruption of Mt. Etna, Sicily, Italy. *Bulletin of Volcanology*, *69*(4), 401–421. <https://doi.org/10.1007/s00445-006-0083-4>
- Corsaro, R. A., & Pompilio, M. (2004). Buoyancy-controlled eruption of magmas at Mt Etna. *Terra Nova*, *16*(1), 16–22. <https://doi.org/10.1046/j.1365-3121.2003.00520.x>
- Corsaro, R. A., Rotolo, S. G., Cocina, O., & Tumbarello, G. (2014). Cognate xenoliths in Mt. Etna lavas: witnesses of the high-velocity body beneath the volcano. *Bulletin of Volcanology*, *76*(1), 772. <https://doi.org/10.1007/s00445-013-0772-8>
- Cristofolini, R., & Romano, R. (1982). Petrologic features of the Etnean volcanic rocks. *Memorie della Società Geologica Italiana*, *23*, 99–115.
- Danyushevsky, L. V., Perfit, M. R., Eggins, S. M., & Falloon, T. J. (2003). Crustal origin for coupled ultra-depleted and plagioclase signatures in MORB olivine-hosted melt inclusions: evidence from the Siqueiros Transform Fault, East Pacific Rise. *Contributions to Mineralogy and Petrology*, *144*(5), 619–637. <https://doi.org/10.1007/s00410-002-0420-3>
- Danyushevsky, L. V., & Plechov, P. (2011). Petrolog3: Integrated software for modeling crystallization processes. *Geochemistry, Geophysics, Geosystems*, *12*, Q07021. <https://doi.org/10.1029/2011GC003516>
- Davis, F. A., Tangeman, J. A., Tennner, T. J., & Hirschmann, M. M. (2009). The composition of KLB-1 peridotite. *American Mineralogist*, *94*(1), 176–180. <https://doi.org/10.2138/am.2009.2984>
- Dixon, J. E. (1997). Degassing of alkalic basalts. *American Mineralogist*, *82*(3-4), 368–378. <https://doi.org/10.2138/am-1997-3-415>
- Dixon, J. E., & Clague, D. A. (2001). Volatiles in basaltic glasses from Loihi Seamount, Hawaii: Evidence for a relatively dry plume component. *Journal of Petrology*, *42*(3), 627–654. <https://doi.org/10.1093/ptrology/42.3.627>
- Dixon, J. E., Stolper, E., & Delaney, J. R. (1988). Infrared spectroscopic measurements of CO₂ and H₂O in Juan de Fuca Ridge basaltic glasses. *Earth and Planetary Science Letters*, *90*(1), 87–104. [https://doi.org/10.1016/0012-821X\(88\)90114-8](https://doi.org/10.1016/0012-821X(88)90114-8)
- Dogliani, C., Innocenti, F., & Mariotti, G. (2001). Why Mt Etna? *Terra Nova*, *13*(1), 25–31. <https://doi.org/10.1046/j.1365-3121.2001.00301.x>
- Elderfield, H. (1986). Strontium isotope stratigraphy. *Palaeogeography, palaeoclimatology, palaeoecology*, *57*(1), 71–90. [https://doi.org/10.1016/0031-0182\(86\)90007-6](https://doi.org/10.1016/0031-0182(86)90007-6)
- Ferlito, C., Viccaro, M., & Cristofolini, R. (2008). Volatile-induced magma differentiation in the plumbing system of Mt. Etna volcano (Italy): evidence from glass in tephra of the 2001 eruption. *Bulletin of Volcanology*, *70*(4), 455–473. <https://doi.org/10.1007/s00445-007-0149-y>
- Ferlito, C., Viccaro, M., Nicotra, E., & Cristofolini, R. (2010). Relationship between the flank sliding of the South East Crater (Mt. Etna, Italy) and the paroxysmal event of November 16, 2006. *Bulletin of Volcanology*, *72*(10), 1179–1190. <https://doi.org/10.1007/s00445-010-0384-5>
- Freda, C., Baker, D. R., & Scarlato, P. (2005). Sulfur diffusion in basaltic melts. *Geochimica et cosmochimica acta*, *69*(21), 5061–5069. <https://doi.org/10.1016/j.gca.2005.02.002>
- Freda, C., Gaeta, M., Misiti, V., Mollo, S., Dolfi, D., & Scarlato, P. (2008). Magma–carbonate interaction: an experimental study on ultra-potassic rocks from Alban Hills (Central Italy). *Lithos*, *101*(3-4), 397–415. <https://doi.org/10.1016/j.lithos.2007.08.008>
- Frezzotti, M. L., Peccerillo, A., & Panza, G. (2009). Carbonate metasomatism and CO₂ lithosphere–asthenosphere degassing beneath the Western Mediterranean: an integrated model arising from petrological and geophysical data. *Chemical Geology*, *262*(1-2), 108–120. <https://doi.org/10.1016/j.chemgeo.2009.02.015>

- Gaeta, M., Di Rocco, T., & Freda, C. (2009). Carbonate assimilation in open magmatic systems: the role of melt-bearing skarns and cumulate-forming processes. *Journal of Petrology*, 50(2), 361–385. <https://doi.org/10.1093/petrology/egp002>
- Gaetani, G. A., O'Leary, J. A., Shimizu, N., Bucholz, C. E., & Newville, M. (2012). Rapid reequilibration of H₂O and oxygen fugacity in olivine-hosted melt inclusions. *Geology*, 40(10), 915–918. <https://doi.org/10.1130/G32992.1>
- Gerlach, T. M. (1991). Present-day CO₂ emissions from volcanos. *Eos, Transactions American Geophysical Union*, 72(23), 249–255.
- Gvirtzman, Z., & Nur, A. (1999). The formation of Mount Etna as the consequence of slab rollback. *Nature*, 401(6755), 782–785. <https://doi.org/10.1038/44555>
- Halmer, M., Schmincke, H.-U., & Graf, H.-F. (2002). The annual volcanic gas input into the atmosphere, in particular into the stratosphere: A global data set for the past 100 years. *Journal of Volcanology and Geothermal Research*, 115(3–4), 511–528. [https://doi.org/10.1016/S0377-0273\(01\)00318-3](https://doi.org/10.1016/S0377-0273(01)00318-3)
- Hartley, M. E., Maclennan, J., Edmonds, M., & Thordarson, T. (2014). Reconstructing the deep CO₂ degassing behaviour of large basaltic fissure eruptions. *Earth and Planetary Science Letters*, 393, 120–131. <https://doi.org/10.1016/j.epsl.2014.02.031>
- Heap, M., Mollo, S., Vinciguerra, S., Lavallée, Y., Hess, K.-U., Dingwell, D. B., et al. (2013). Thermal weakening of the carbonate basement under Mt. Etna volcano (Italy): Implications for volcano instability. *Journal of Volcanology and Geothermal Research*, 250, 42–60. <https://doi.org/10.1016/j.jvolgeores.2012.10.004>
- Helo, C., Longpré, M.-A., Shimizu, N., Clague, D. A., & Stix, J. (2011). Explosive eruptions at mid-ocean ridges driven by CO₂-rich magmas. *Nature Geoscience*, 4(4), 260–263. <https://doi.org/10.1038/ngeo1104>
- Hirn, A., Nercessian, A., Sapin, M., Ferrucci, F., & Wittlinger, G. (1991). Seismic heterogeneity of Mt Etna: structure and activity. *Geophysical Journal International*, 105(1), 139–153. <https://doi.org/10.1111/j.1365-246X.1991.tb03450.x>
- Jennings, E. S., & Holland, T. J. (2015). A simple thermodynamic model for melting of peridotite in the system NCFMASOCr. *Journal of Petrology*, 56(5), 869–892. <https://doi.org/10.1093/petrology/egv020>
- Jennings, E. S., Holland, T. J., Shorttle, O., Maclennan, J., & Gibson, S. A. (2016). The composition of melts from a heterogeneous mantle and the origin of ferropicrite: Application of a thermodynamic model. *Journal of Petrology*, 57(11–12), 2289–2310.
- Jochum, K. P., Nohl, U., Herwig, K., Lammel, E., Stoll, B., & Hofmann, A. W. (2005). GeoReM: A new geochemical database for reference materials and isotopic standards. *Geostandards and Geoanalytical Research*, 29(3), 333–338. <https://doi.org/10.1111/j.1751-908X.2005.tb00904.x>
- Jochum, K. P., Weis, U., Stoll, B., Kuzmin, D., Yang, Q., Raczek, I., et al. (2011). Determination of reference values for NIST SRM 610–617 glasses following ISO guidelines. *Geostandards and Geoanalytical Research*, 35(4), 397–429. <https://doi.org/10.1111/j.1751-908X.2011.00120.x>
- Kahl, M., Viccaro, M., Ubide, T., Morgan, D. J., & Dingwell, D. B. (2017). A branched magma feeder system during the 1669 eruption of Mt Etna: Evidence from a time-integrated study of zoned olivine phenocryst populations. *Journal of Petrology*, 58(3), 443–472. <https://doi.org/10.1093/petrology/egx022>
- Kamenetsky, V., & Clocchiatti, R. (1996). Primitive magmatism of Mt. Etna: Insights from mineralogy and melt inclusions. *Earth and Planetary Science Letters*, 142(3–4), 553–572. [https://doi.org/10.1016/0012-821X\(96\)00115-X](https://doi.org/10.1016/0012-821X(96)00115-X)
- Kamenetsky, V. S., Pompilio, M., Métrich, N., Sobolev, A. V., Kuzmin, D. V., & Thomas, R. (2007). Arrival of extremely volatile-rich high-Mg magmas changes explosivity of Mount Etna. *Geology*, 35(3), 255–258. <https://doi.org/10.1130/G23163A.1>
- Katz, R. F., Spiegelman, M., & Langmuir, C. H. (2003). A new parameterization of hydrous mantle melting. *Geochemistry, Geophysics, Geosystems*, 4(9), 1073. <https://doi.org/10.1029/2002GC000433>
- Kogiso, T., Hirose, K., & Takahashi, E. (1998). Melting experiments on homogeneous mixtures of peridotite and basalt: Application to the genesis of ocean island basalts. *Earth and Planetary Science Letters*, 162(1–4), 45–61. [https://doi.org/10.1016/S0012-821X\(98\)00156-3](https://doi.org/10.1016/S0012-821X(98)00156-3)
- Koleszar, A. M., Saal, A. E., Hauri, E. H., Nagle, A. N., Liang, Y., & Kurz, M. D. (2009). The volatile contents of the Galapagos plume: Evidence for H₂O and F open system behavior in melt inclusions. *Earth and Planetary Science Letters*, 287(3–4), 442–452. <https://doi.org/10.1016/j.epsl.2009.08.029>
- Maclennan, J. (2017). Bubble formation and decrepitation control the CO₂ content of olivine-hosted melt inclusions. *Geochemistry, Geophysics, Geosystems*, 18, 597–616. <https://doi.org/10.1002/2016GC006633>
- Maclennan, J., McKenzie, D., Hilton, F., Gronvöld, K., & Shimizu, N. (2003). Geochemical variability in a single flow from northern Iceland. *Journal of Geophysical Research*, 108(B1), 2007. <https://doi.org/10.1029/2000JB000142>
- Mangan, M., & Sisson, T. (2000). Delayed, disequilibrium degassing in rhyolite magma: decompression experiments and implications for explosive volcanism. *Earth and Planetary Science Letters*, 183(3–4), 441–455. [https://doi.org/10.1016/S0012-821X\(00\)00299-5](https://doi.org/10.1016/S0012-821X(00)00299-5)
- Marty, B., Trull, T., Lussiez, P., Basile, I., & Tanguy, J.-C. (1994). He, Ar, O, Sr and Nd isotope constraints on the origin and evolution of Mount Etna magmatism. *Earth and Planetary Science Letters*, 126(1–3), 23–39. [https://doi.org/10.1016/0012-821X\(94\)90240-2](https://doi.org/10.1016/0012-821X(94)90240-2)
- Marziano, G. I., Gaillard, F., & Pichavant, M. (2008). Limestone assimilation by basaltic magmas: An experimental re-assessment and application to Italian volcanoes. *Contributions to Mineralogy and Petrology*, 155(6), 719–738. <https://doi.org/10.1007/s00410-007-0267-8>
- Mason, E., Edmonds, M., & Turchyn, A. V. (2017). Remobilization of crustal carbon may dominate volcanic arc emissions. *Science*, 357(6348), 290–294. <https://doi.org/10.1126/science.aan5049>
- Matthews, S., Shorttle, O., Rudge, J. F., & Maclennan, J. (2017). Constraining mantle carbon: CO₂-trace element systematics in basalts and the roles of magma mixing and degassing. *Earth and Planetary Science Letters*, 480, 1–14. <https://doi.org/10.1016/j.epsl.2017.09.047>
- McDonough, W. F., & Sun, S.-S. (1995). The composition of the Earth. *Chemical geology*, 120(3–4), 223–253. [https://doi.org/10.1016/0009-2541\(94\)00140-4](https://doi.org/10.1016/0009-2541(94)00140-4)
- Métrich, N., Allard, P., Spilliaert, N., Andronico, D., & Burton, M. (2004). 2001 flank eruption of the alkali-and volatile-rich primitive basalt responsible for Mount Etna's evolution in the last three decades. *Earth and Planetary Science Letters*, 228(1–2), 1–17. <https://doi.org/10.1016/j.epsl.2004.09.036>
- Métrich, N., & Clocchiatti, R. (1989). Melt inclusion investigation of the volatile behaviour in historic alkali basaltic magmas of Etna. *Bulletin of Volcanology*, 51(3), 185–198. <https://doi.org/10.1007/BF01067955>
- Métrich, N., & Clocchiatti, R. (1996). Sulfur abundance and its speciation in oxidized alkaline melts. *Geochimica et Cosmochimica Acta*, 60(21), 4151–4160. [https://doi.org/10.1016/S0016-7037\(96\)00229-3](https://doi.org/10.1016/S0016-7037(96)00229-3)
- Métrich, N., & Wallace, P. J. (2008). Volatile Abundances in Basaltic Magmas and Their Degassing Paths Tracked by Melt Inclusions. *Reviews in Mineralogy and Geochemistry*, 69(1), 363–402. <https://doi.org/10.2138/rmg.2008.69.10>
- Michaud, V. (1995). Crustal xenoliths in recent hawaiiites from Mount Etna, Italy: evidence for alkali exchanges during magma-wall rock interaction. *Chemical Geology*, 122(1–4), 21–42. [https://doi.org/10.1016/0009-2541\(94\)00133-S](https://doi.org/10.1016/0009-2541(94)00133-S)
- Mollo, S., Gaeta, M., Freda, C., Di Rocco, T., Misiti, V., & Scarlato, P. (2010). Carbonate assimilation in magmas: A reappraisal based on experimental petrology. *Lithos*, 114(3–4), 503–514. <https://doi.org/10.1016/j.lithos.2009.10.013>

- Montelli, R., Nolet, G., Dahlen, F., & Masters, G. (2006). A catalogue of deep mantle plumes: New results from finite-frequency tomography. *Geochemistry, Geophysics, Geosystems*, 7, Q1100. <https://doi.org/10.1029/2006GC001248>
- Moore, G. (2008). Interpreting H₂O and CO₂ contents in melt inclusions: constraints from solubility experiments and modeling. *Reviews in Mineralogy and Geochemistry*, 69(1), 333–362. <https://doi.org/10.2138/rmg.2008.69.9>
- Mulas, M., Cioni, R., Andronico, D., & Mundula, F. (2016). The explosive activity of the 1669 Monti Rossi eruption at Mt. Etna (Italy). *Journal of Volcanology and Geothermal Research*, 328, 115–133. <https://doi.org/10.1016/j.jvolgeores.2016.10.012>
- Neave, D. A., Maclennan, J., Edmonds, M., & Thordarson, T. (2014). Melt mixing causes negative correlation of trace element enrichment and CO₂ content prior to an Icelandic eruption. *Earth and Planetary Science Letters*, 400, 272–283. <https://doi.org/10.1016/j.epsl.2014.05.050>
- Newman, S., & Lowenstern, J. B. (2002). VolatileCalc: a silicate melt–H₂O–CO₂ solution model written in Visual Basic for excel. *Computers & Geosciences*, 28(5), 597–604. [https://doi.org/10.1016/S0098-3004\(01\)00081-4](https://doi.org/10.1016/S0098-3004(01)00081-4)
- Patanè, D., Barberi, G., Cocina, O., De Gori, P., & Chiarabba, C. (2006). Time-resolved seismic tomography detects magma intrusions at Mount Etna. *Science*, 313(5788), 821–823. <https://doi.org/10.1126/science.1127724>
- Patanè, D., Privitera, E., Gresta, S., Alparone, S., Akinci, A., Barberi, G., et al. (2003). Seismological constraints for the dyke emplacement of the July–August 2001 lateral eruption at Mt. Etna volcano, Italy. *Annals of Geophysics*, 46(4).
- Pedley, H. M., & Grasso, M. (1992). Miocene syntectonic sedimentation along the western margins of the Hyblean–Malta platform: a guide to plate margin processes in the central Mediterranean. *Journal of Geodynamics*, 15(1–2), 19–37. [https://doi.org/10.1016/0264-3707\(92\)90004-C](https://doi.org/10.1016/0264-3707(92)90004-C)
- Pichavant, M., Di Carlo, I., Le Gac, Y., Rotolo, S. G., & Scaillet, B. (2009). Experimental constraints on the deep magma feeding system at Stromboli volcano, Italy. *Journal of Petrology*, 50(4), 601–624. <https://doi.org/10.1093/petrology/egp014>
- Pichavant, M., Di Carlo, I., Rotolo, S. G., Scaillet, B., Burgisser, A., Le Gall, N., & Martel, C. (2013). Generation of CO₂-rich melts during basalt magma ascent and degassing. *Contributions to Mineralogy and Petrology*, 166(2), 545–561. <https://doi.org/10.1007/s00410-013-0890-5>
- Roeder, P. L., & Emslie, R. F. (1970). Olivine-liquid equilibrium. *Contributions to Mineralogy and Petrology*, 29(4), 275–289. <https://doi.org/10.1007/BF00371276>
- Ryan, W. B., Carbotte, S. M., Coplan, J. O., O'Hara, S., Melkonian, A., Arko, R. A., et al. (2009). Global multi-resolution topography synthesis. *Geochemistry, Geophysics, Geosystems*, 10, Q03014. <https://doi.org/10.1029/2008GC002332>
- Saal, A. E., Hauri, E. H., Langmuir, C. H., & Perfit, M. R. (2002). Vapour undersaturation in primitive mid-ocean-ridge basalt and the volatile content of Earth's upper mantle. *Nature*, 419(6906), 451–455. <https://doi.org/10.1038/nature01073>
- Schiano, P., Clocchiatti, R., Ottolini, L., & Busa, T. (2001). Transition of Mount Etna lavas from a mantle-plume to an island-arc magmatic source. *Nature*, 412(6850), 900–904. <https://doi.org/10.1038/35091056>
- Schiavi, F., Rosciglione, A., Kitagawa, H., Kobayashi, K., Nakamura, E., Nuccio, P. M., et al. (2015). Geochemical heterogeneities in magma beneath Mount Etna recorded by 2001–2006 melt inclusions. *Geochemistry, Geophysics, Geosystems*, 16, 2109–2126. <https://doi.org/10.1002/2015GC005786>
- Shaw, A. M., Behn, M. D., Humphris, S. E., Sohn, R. A., & Gregg, P. M. (2010). Deep pooling of low degree melts and volatile fluxes at the 85 E segment of the Gakkel Ridge: Evidence from olivine-hosted melt inclusions and glasses. *Earth and Planetary Science Letters*, 289(3–4), 311–322. <https://doi.org/10.1016/j.epsl.2009.11.018>
- Shishkina, T. A., Botcharnikov, R. E., Holtz, F., Almeev, R. R., Jazwa, A. M., & Jakubiak, A. A. (2014). Compositional and pressure effects on the solubility of H₂O and CO₂ in mafic melts. *Chemical Geology*, 388, 112–129. <https://doi.org/10.1016/j.chemgeo.2014.09.001>
- Sides, I. R., Edmonds, M., Maclennan, J., Swanson, D. A., & Houghton, B. F. (2014). Eruption style at Kilauea Volcano in Hawai'i linked to primary melt composition. *Nature Geoscience*, 7(6), 464–469. <https://doi.org/10.1038/ngeo2140>
- Sobolev, A., & Nikogosian, I. (1994). Petrology of long-lived mantle plume magmatism: Hawaii, Pacific and Reunion Island, Indian Ocean. *Petrology*, 2(2), 111–144.
- Sobolev, A. V., Hofmann, A. W., & Nikogosian, I. K. (2000). Recycled oceanic crust observed in 'ghost plagioclase' within the source of Mauna Loa lavas. *Nature*, 404(6781), 986–990. <https://doi.org/10.1038/35010098>
- Soule, S. A., Nakata, D. S., Fornari, D. J., Fundis, A. T., Perfit, M. R., & Kurz, M. D. (2012). CO₂ variability in mid-ocean ridge basalts from syn-emplacement degassing: Constraints on eruption dynamics. *Earth and Planetary Science Letters*, 327–328, 39–49.
- Spilliaert, N., Allard, P., Métrich, N., & Sobolev, A. (2006). Melt inclusion record of the conditions of ascent, degassing, and extrusion of volatile-rich alkali basalt during the powerful 2002 flank eruption of Mount Etna (Italy). *Journal of Geophysical Research*, 111, B04203. <https://doi.org/10.1029/2005JB003934>
- Spilliaert, N., Métrich, N., & Allard, P. (2006). S–Cl–F degassing pattern of water-rich alkali basalt: Modelling and relationship with eruption styles on Mount Etna volcano. *Earth and Planetary Science Letters*, 248(3–4), 772–786. <https://doi.org/10.1016/j.epsl.2006.06.031>
- Tanguy, J., & Kieffer, G. (1977). The 1974 eruption of Mount Etna. *Bulletin Volcanologique*, 40(4), 239–252. <https://doi.org/10.1007/BF02597566>
- Tanguy, J., Kieffer, G., & Patanè, G. (1996). Dynamics, lava volume and effusion rate during the 1991–1993 eruption of Mount Etna. *Journal of Volcanology and Geothermal Research*, 71(2–4), 259–265. [https://doi.org/10.1016/0377-0273\(95\)00081-X](https://doi.org/10.1016/0377-0273(95)00081-X)
- Tanguy, J.-C., Condomines, M., & Kieffer, G. (1997). Evolution of the Mount Etna magma: constraints on the present feeding system and eruptive mechanism. *Journal of Volcanology and Geothermal research*, 75(3–4), 221–250. [https://doi.org/10.1016/S0377-0273\(96\)00065-0](https://doi.org/10.1016/S0377-0273(96)00065-0)
- Venezky, D., & Rutherford, M. (1997). Preeruption conditions and timing of dacite-andesite magma mixing in the 2.2 ka eruption at Mount Rainier. *Journal of Geophysical Research*, 102(B9), 20,069–20,086. <https://doi.org/10.1029/97JB01590>
- Viccaro, M., & Cristofolini, R. (2008). Nature of mantle heterogeneity and its role in the short-term geochemical and volcanological evolution of Mt. Etna (Italy). *Lithos*, 105(3–4), 272–288. <https://doi.org/10.1016/j.lithos.2008.05.001>
- Viccaro, M., Ferlito, C., Cortesogno, L., Cristofolini, R., & Gaggero, L. (2006). Magma mixing during the 2001 event at Mount Etna (Italy): Effects on the eruptive dynamics. *Journal of Volcanology and Geothermal Research*, 149(1–2), 139–159. <https://doi.org/10.1016/j.jvolgeores.2005.06.004>
- Wallace, P. J., Kamenetsky, V. S., & Cervantes, P. (2015). Melt inclusion CO₂ contents, pressures of olivine crystallization, and the problem of shrinkage bubbles. *American Mineralogist*, 100(4), 787–794. <https://doi.org/10.2138/am-2015-5029>
- Witham, F., Blundy, J., Kohn, S. C., Lesne, P., Dixon, J., Churakov, S. V., & Botcharnikov, R. (2012). SolEx: A model for mixed COHSLI-volatile solubilities and exsolved gas compositions in basalt. *Computers & Geosciences*, 45, 87–97. <https://doi.org/10.1016/j.cageo.2011.09.021>

- Woods, A. W., & Cardoso, S. S. (1997). Triggering basaltic volcanic eruptions by bubble-melt separation. *Nature*, 385(6616), 518–520. <https://doi.org/10.1038/385518a0>
- Workman, R. K., Hauri, E., Hart, S. R., Wang, J., & Blusztajn, J. (2006). Volatile and trace elements in basaltic glasses from Samoa: Implications for water distribution in the mantle. *Earth and Planetary Science Letters*, 241(3–4), 932–951. <https://doi.org/10.1016/j.epsl.2005.10.028>
- Zajacz, Z. (2015). The effect of melt composition on the partitioning of oxidized sulfur between silicate melts and magmatic volatiles. *Geochimica et Cosmochimica Acta*, 158, 223–244. <https://doi.org/10.1016/j.gca.2015.01.036>